A survey of the neutral atomic hydrogen in M33

Deul, E.R.; Hulst, J.M. van der

ASTRONOMY & ASTROPHYSICS
SUPPLEMENT SERIES

FEBRUARY **1987,** PAGE 509

Astron. Astrophys. Suppl. Ser. **67,** 509-539 (1987)

A survey of the neutral atomic hydrogen in M33

E. R. Deul ([1]) and J. M. van der Hulst ([2])

([1]) Sterrewacht Leiden, Postbus 9513, NL-2300 RA Leiden, The Netherlands
([2]) Netherlands Foundation for Radio Astronomy, Postbus 2, NL-7990 AA Dwingeloo, The Netherlands

Received March 19, accepted June 2, 1986

Summary. — We present a survey of the 21-cm line of HI in M33, carried out with the Westerbork Synthesis Radio Telescope at a resolution of $12'' \times 24''$ (ra × dec.), corresponding to $\sim 40 \times 40$ pc in the plane of this galaxy, and at a velocity resolution of 8.2 km s^{-1}. The non-standard reduction techniques are extensively described, especially those involving the addition of short-baseline information from Effelsberg 100-m observations and the extrapolation of these baselines using the method of Braun and Walterbos. The survey is displayed in various formats as radio photographs with grey scales and contours in order to emphasize the continuity along all axes of the data cube. A short description of some of the most striking features in the channel maps is given. In addition to the fine-scale structure shown by filamentary and shell-like regions and by regions that seem devoid of HI emission, large scale, extended structures giving rise to double profiles can also be seen. The latter distributions are most probably caused by the warped outer HI layer. Anomalous velocities especially at the position of the optical spiral arms are also present.

Key words : galaxies : M33 ; kinematics and dynamics of ; structure of — interferometry — interstellar medium : kinematics and dynamics — radio lines : 21-cm.

1. Introduction.

Due to its favourable inclination ($i = 55°$) and large angular extent ($53' \times 83'$; Holmberg, 1950) M33 (the Triangulum Nebula, NGC 598) is well suited for studies of the fine-scale structure and kinematics of its interstellar medium. Table I presents some general information on M33. This galaxy is a late-type spiral (Sc) having an overall relatively high projected surface density of neutral hydrogen, which makes it possible to detect small-scale structures with a good signal-to-noise ratio. The proximity of M33 (724 kpc, Madore *et al.*, 1985) enables the Westerbork Synthesis Radio Telescope (WSRT) to reach down to sizes as small as 40 parsecs, the domain of the giant molecular clouds, HII regions, OB associations, and evolved supernova remnants.

Since its first detection in HI by Volders in 1957, M33 has been observed frequently. A list of all neutral hydrogen observations made before our work is given in table II. The present survey was carried out using the 3-km Westerbork array. The new observations represent a factor of four improvement in sensitivity and angular resolution compared with the best previous work (Cambridge survey by Newton and Reakes, 1980). The WSRT data cover most of the optical part of M33, with a resolution of $\delta(\mathrm{Ra}) \times \delta(\mathrm{Dec}) \times \delta(V) = 12'' \times 24'' \times 8.2$ km s^{-1}. In order to incorporate short spacing data missing from the WSRT material, W. Huchtmeier of the Max-Planck Institut für Radioastronomie has kindly made available Effelsberg 100-m single dish observations.

This paper describes the various stages of the reduction process, presents the survey in a compressed form and discusses some of the striking characteristics of the HI in M33. The complete interpretation of the data will be given elsewhere. Section 2 outlines the observational parameters of the survey. Section 3 is devoted to a discussion of the non-standard methods employed during the reduction process. The reduced data are presented in various formats in section 4. Section 5 briefly discusses some outstanding features. Finally appendix A presents a comparison between the two methods used to fill in the short-spacing information.

2. The observations.

In its present configuration the WSRT consists of a 14 element array occupying roughly a 3 km long baseline. Four telescopes are movable and these are cross-correlated with the other ten telescopes yielding 40 baselines per 12-hour observation. A full synthesis involves four 12-hour observing runs with a resulting uniform baseline coverage from 36 to 2772 meters at 18 meter spacings, resulting in the first grating ring at a distance of $\sim 40'$ from the fringe stopping center. The basic instrumental properties have been thoroughly described by Baars and Hooghoudt (1974), Casse and Muller (1974), Högbom and Brouw (1974), Brouw (1975) and Bos *et al.* (1981).

Because M33 has a large angular extent — roughly $0.^{\circ}9 \times 1.^{\circ}5$ — one full synthesis field is not enough to

Send offprint requests to : E. R. Deul.

cover fully the optical image. Therefore two fields were observed. The south-eastern field was centred on the prominent southern arm, just below the nucleus of M33. The north-western field was chosen such that the resulting combined primary beam is evenly distributed over the optical image of M33. Figure 1 shows the two-field centers together with their halfpower beams superimposed on a Palomar sky survey blue plate reproduction. The type of the galaxy and its mass yield a rather low rotational velocity. In addition the inclination of 55° (0° is face on) causes the radial velocity extent to be reduced by a factor 0.8. Therefore we did not need a wide frequency band to cover the kinematic extent of M33. For each field 64 channels, separated by 4.12 km s^{-1}, are sufficient to span the velocity width in the part of the galaxy covered by each halfpower beam. The heliocentric velocities for the central passbands were chosen accordingly, keeping in mind that the two fields had to be added later on in the reduction process. The two velocity grids have a central velocity difference of 20 channel widths. Table III gives the observational parameters for each field separately and lists the properties of the WSRT used in this survey.

The standard WSRT calibration package was used by the Dwingeloo reduction group to calibrate the observations. A discussion of this procedure is given by van Someren Greve (1974) and by Bos *et al.* (1981). The calibration sources, usually observed for a few hours prior to or right after the synthesis observations are the three standard ones : 3C147, 3C286, and 3C309.1 (see Tab. IV).

M33 is situated rather far from the galactic plane ($l = 133\overset{\circ}{.}69$, $b = -31\overset{\circ}{.}35$) at a velocity range ($\sim -320$ to ~ -55 km s^{-1}) which does not coincide with that of our own Galaxy, consequently there is no contamination from foreground HI emission. This can be seen in figure 2, where we have plotted the observed single-dish Dwingeloo 25-m spectrum taken at the north-western field position. The foreground Milky Way HI manifests itself as a dip in the profile at the high velocity side of the emission from M33, because of the beam switching technique used. The Westerbork maps at the high velocity side of the passband also do not show any contaminating foreground HI emission.

3. Reduction.

In addition to the standard Westerbork reduction procedure described briefly in this section, we describe the Braun-Walterbos technique (1985) for extrapolating short spacing information from the existing WSRT data and compared the results of this technique with the method of adding observed short-spacing data.

3.1 CORRECTING FOR MISSING SHORT SPACINGS. — The baseline coverage of the WSRT is restricted to a minimum spacing of 36 meters and a maximum spacing of 2772 meters. The individual increment is 18 meters. Therefore the *u-v* coverage of the WSRT is incomplete at the 0 and 18 meters intervals. This incompleteness causes a central zero level depression in the synthesized beam. The change of the zero level in a map depends on the location and intensity of emission present. There are several ways to correct for this effect. One way involves incorporating observations made with a different instrument that does include the 0- and 18-meter spacings. One such instrument is the 100-m Effelsberg telescope of the Max-Planck Institut für Radioastronomie. M33 has been surveyed with this instrument by Huchtmeier (1973). These observations were, however, sampled over an area of roughly $3\overset{\circ}{.}0 \times 2\overset{\circ}{.}7$ every $0\overset{\circ}{.}25 \times 0\overset{\circ}{.}15$ with a beam of 0°15 FWHM, resulting in severe undersampling. The consequence of spatial undersampling is aliasing in the *u-v* plane, which makes it impossible to derive correct values for the 0- and 18-meter baselines (Bajaja and van Albada, 1978). At our request W. Huchtmeier kindly reobserved M33 on a denser grid, but, because of limited observing time, only over a smaller area. This new, fully sampled survey is confined to a $0\overset{\circ}{.}75 \times 0\overset{\circ}{.}75$ area, thus missing the outer parts of M33. Therefore correct incorporation of the 0- and 18-meter spacings can only be done in those channels where most of the HI emission is within the fully sampled area. This is the case for 22 maps in the velocity range of ~ -212 to ~ -125 km s^{-1}, but even for the channel map at the systemic velocity weak HI emission can be found outside the Effelsberg fully-sampled region. Therefore we have merged the new Huchtmeier data with the old, undersampled survey. Both Effelsberg surveys were checked for internal calibration ; a consistancy to within 1 % was found. Aliasing is not a problem, because the contribution of the undersampled emission to a given map is rather small. For the given velocity interval the Effelsberg 100-m spectra were convolved to the WSRT channel width and separation, sorted, and used to create channel maps. These maps were then regridded to both WSRT fields. A fast Fourier transform was used to extract the 0- and 18- meter spacing visibilities, which were then incorporated into the WSRT interferometer data during its fast Fourier transform to channel maps. Figures 3(a) and 3(d) show a typical example of two maps without short spacing information ; the central depression is clearly visible around the emission region. Figures 3(b) and 3(e) have the 0- and 18-meter data incorporated. All maps were smoothed to eight times the original resolution to emphasize the large scale spatial variations. The box depicts the area of fully sampled Effelsberg observations. Below each map a vertical cross-cut through the map is presented, showing a flat zero level in the maps which incorporate the short spacing information.

The calibration of the Effelsberg 100-m observations with respect to the WSRT data, has been carried out by comparing the observed 36-m spacing of the WSRT with the 36-m spacing data extracted from the Effelsberg data. Figure 4 shows a plot of both sets of 36-meter data. The amplitudes agree to within 5 %. The phases differ by less than 10°. The procedure described above could be applied successfully only for channel maps at velocities between -211.8 and -125.3 km s^{-1}. Because no fully sampled short spacing data are available for the more extreme velocities the remaining channels were processed differently, using extrapolation from the existing WSRT data. One such method has been described by Braun and

Walterbos (1985). Because this method gives the best results and is easy to use. The method can only be applied if enough map plane area between the extended emission and the first grating ring radius can be assumed to be free of emission. In practice, this means that the emission region should be smaller than about 75 % of the first grating ring radius (Braun and Walterbos, 1985). Maps that do not satisfy this constraint could be processed using the Effelsberg data. All maps subject to the Braun-Walterbos technique were first reduced in pixel dimensions using a Kappa-Sigma clipping routine (Herzog and Illingworth, 1977). Each map was inspected on the Leiden image processing display in order to identify and then mask out all areas containing extended emission or grating rings. Finally for each map a Fourier fit was determined and this fit was subtracted from the full resolution map. Figures 3(a), 3(c), 3(d) and 3(f) show a typical example of two maps before and after applying the Braun-Walterbos procedure. The examples shown are included for comparison with the correction derived from the single dish data. These are not the best examples to illustrate the Braun-Walterbos method, however, because the emission region is larger than 75 % of the first grating ring radius in the right ascension direction, resulting in some confusion between emission and grating rings. The vertical cross-cuts through these maps plotted below each map show constant zero levels for the corrected maps. They also show, however, that even in these cases the bowl is satisfactorily removed. Appendix A presents a detailed comparison between the results of the Braun-Walterbos method and the more familiar one based on incorporation of single-dish data, as well as the criterion on which the choice of technique is based. To ensure continuity we gradually changed the influence of one method compared to the other by weighting the channel maps. The boundary channels contain an equal amount of short spacing information determined by both methods. The neighboring channels inside these boundaries were weighted 3/4 with short-spacing information from Effelsberg data and 1/4 with short-spacing data obtained via the Braun-Walterbos technique ; the neighboring channels outside the boundaries were weighted the other way around.

3.2 CLEANING. — The absence of some interferometer data in small intervals in hour angle due to the malfunction of telescopes and the deletion of unreliable correlations caused slight imperfections that make cleaning of the maps necessary. The sidelobe amplitude of the beam in both fields amounts to a few percent of the main lobe. We used the cleaning method described by Högbom (1974), Harten (1974), and Schwarz (1978). All maps including the short spacing information were decomposed into delta components over an area as large as necessary (typically 512 × 440 pixels) to a level of about 4 times the noise in that map. The components found in this way were then removed using the synthesized beam pattern, which includes short spacings. We restored these components with the central lobe of the same beam pattern on the residual map. For each field the continuum map was cleaned over the identical area as the corresponding channel map. This was done because the antenna pattern of a given channel map differs from the antenna pattern of the continuum map, due to different u-v frequencies in the Fourier transformation (see Sect. 3.3).

3.3 CONTINUUM SUBTRACTION. — In order to subtract continuum radiation from the line emission we used a continuum map constructed from the line survey by adding (separately for each field) all channels that were judged free from line emission. The velocity width of the line emission was determined using Dwingeloo 25-m single dish observations at both field centers. Because the velocity range of the HI in M33 is larger than a single WSRT passband, at the resolution used $(\sim 258.3 \text{ km s}^{-1})$ we shifted the central velocities such that one side of the passband in either field would contain enough channel maps without line emission to allow construction of the continuum map. At the low-velocity edge of the passband one or two channels contained DC offset rings centred on the fringe stopping center and are thus of no use. At the high-velocity side of the passband four to five channels had to be excluded from further reduction because they are so close to the edge of the band and are unstable and very noisy.

In this way we constructed two continuum maps, one for the high-velocity side (south western field) made from 5 channel maps at velocities -55.3 through -34.7 km s^{-1} and one for the low-velocity side (north-eastern field) made from 9 channel maps at velocities -355.6 through -330.9 km s^{-1}.

We checked our assumption of a flat velocity baseline by comparing the fluxes of strong point sources in both continuum maps. The difference in their fluxes is less than 4 %.

We have determined the position and relative fluxes of strong sources in the fields and subtracted them in the u-v plane from all velocities, including the HI free channels. This was done because the channel maps were Fourier transformed in blocks of eight channels using the average observed u-v frequency per block. It was necessary to work in this way because each channel has its corresponding observed u-v frequency. If we were to use only one u-v frequency for all channel maps, then the position of point sources would change with velocity, and their grating rings would have equal diameters. Using different u-v frequencies causes the grating rings to have different sizes, but point sources are stationary in velocity. The observed u-v frequency determines the baseline values in wavelengths. A Fourier transformation in blocks causes detectable displacements. This results in problems with strong point sources near the edge of the field, because their grating rings will cross HI line emission in the center of the map and cannot be subtracted accurately using the continuum maps. Therefore we have determined the position and relative fluxes of these strong background sources (see Tab. VI) and subtracted them in the u-v plane, for all velocities including the HI free channels.

3.4 CREATION OF THE DATA CUBE. — The next step in the reduction process involved the combination of the two different fields. The fields were observed with

different fringe stopping centers and have different coordinate grids. Before adding these fields we regridded them to a WSRT coordinate system centred on the nucleus of M33. In order to optimize the S/N ratio, which depends on the distance from the fringe stopping center, both fields were weighted with their primary-beam attenuation before the addition (Brinks, 1984) and a rough mask was constructed to isolate the region of interest. The primary-beam attenuation is approximately Gaussian in form with a half power width of 36′5. The analytical expression used for the attenuation is :

$$F(r) = 99.75 \times \exp\left(-2.680\, r^2 - 0.362\, r^4 - 0.192\, r^6\right) + 0.25 ,$$

where r is the distance in degrees from the fringe stopping center. After combination the primary-beam weighting was corrected to obtain channel maps with equal noise over the whole map. Primary beam corrected channel maps were created by again correcting above-mentioned maps with the primary beam. All equal-noise channel maps were smoothed to eight times the original resolution. A single contour was constructed at 1.5 times the noise level in these maps and spurious peaks were taken out by manual inspection of the data for discontinuities in velocity and/or spacial coordinates. All channel maps were masked using these single contours, resulting in maps that only show areas with significant line emission. These maps were used to construct a column density map by summing over all velocities. At the same time a velocity map and a map of the velocity width were made, utilizing the parameters of a Gaussian least squares fit to the velocity profiles.

4. The results.

The final data set at full resolution contains 66 channel maps each with 1024 × 1024 pixels. We plotted each map as a radio photograph using both grey scales and contours. The 66 channels were processed in the same way, resulting in a homogeneous set of data. Because two fields were combined the noise varies across the maps ; it is the highest at the north-eastern and south-western edges. The synthesized beam is depicted in the lower righthand corner of each panel in figures 5 ; the heliocentric velocity is indicated in the top right hand corner of each frame. The intensities displayed range from 1.2 K at the noise level to 96.0 K at maximum intensity. The plots are presented on as large a scale as possible in order to show the fine scale structure of the HI gas in M33. To enhance the extended low brightness structure we have plotted the grey scales using a smoothed version of the contour map (resolution 24″ × 48″). Only the even numbered channel are presented, because of constraints on the publication. The separation is therefore 8.2 km s^{-1} equal to the Hanning-tapered resolution.

Surveys of the present sort involve a three dimensional cube of data. The two-dimensional channel maps do not reveal regularities in the velocity coordinate ; to show this, an additional set of maps is necessary. Figures 6 and 7 show plots of brightness temperature as a function of position and velocity along cuts through M33. Crosscuts through the full-resolution maps would result in a large number of maps, therefore we smoothed the original channel maps to a lower resolution of 24″ × 48″. Figure 6 shows crosscuts perpendicular to the minor axis, spaced at regular intervals of 0′8 along the minor axis ; figure 7 shows cuts perpendicular to the major axis, spaced at 2′4 intervals. Therefore the resolution of the figure 6 is 0′8 × 8.2 km s^{-1} ; the resolution of the figure 7 maps is 2′4 × 8.2 km s^{-1}. The position of each crosscut is given by its perpendicular distance from the major axis for figure 6 and from the minor axis for figure 7 at the top righthand corner of each panel, using the points of the compass as the sense of direction. These maps are also presented in grey scale and contours to display the data in a quantitative way. Again, only half of the available position-velocity maps are presented, because of publication constraints.

Figure 8 shows the column density map of HI in M33. The synthesized beam size is indicated in the bottom right-hand corner. The map is corrected for primary beam attenuation ; consequently the noise level is not uniform, being highest in the south-eastern and north-western parts. Notice the asymmetry between the northern and southern hemispheres. Because the position angle of M33 is small and its declination is close to 30°, a deprojected surface brighness map would seem to have been observed with an almost circular beam, therefore the resolution in the plane of M33 is circular (40 × 40 pc).

Figure 9 shows the velocity field of the HI gas in M33. Figure 10 shows a plot of the radial HI distribution as calculated from the deprojected hydrogen surface density map by averaging the intensities in radial intervals centred on the nucleus of M33. A central depression extending to 1 kpc can be seen in figure 10, together with the signature of spiral structure giving the sawtooth like appearance between 1 and 6 kpc radii. The sharp decay of the apparent column density at radii beyond 6 kpc is caused by the extreme warp of the outer HI layer in M33.

5. Discussion.

Only a brief discussion of some of the most striking features of the HI distribution in M33 will be given here. A detailed analysis of the data is in progress and will be reported elsewhere.

5.1 THE LARGE SCALE STRUCTURE. — The position-velocity plot along the major axis of M33 shows the expected signature of differential rotation. The gradual increase in rotation velocity with radius is typical for a late type galaxy (Bosma, 1981 ; Wevers, 1984). The large scale regularity in velocity can also be seen in the figure 9 velocity-field map. If one examines the velocity field closely, however, in particular some of the position-velocity plots parallel to the minor axis, there are several regions where double profiles are observed (see the Fig. 6 profiles at 9′6 through 16′0 distances at 20′ north and at − 16′0 through − 9′6 distances at − 20′ south of the nucleus of M33). This has already been discussed by Rogstad *et al.* (1976), but our higher resolution data will

enable us to pursue these anomalous velocities in detail. Double profiles can be understood as due to an extremely warped hydrogen distribution. The low-brightness emission regions that can be seen in the channel maps close to the systemic velocity, well outside the major emitting disk, also are the result of a warped component. We are currently in the process of fitting a flaring, warped hydrogen layer model (Brinks and Burton, 1984) to the observations.

Indications of a shift in position angle of the major axis with radius in the disk of M33 can be seen from the channel maps at the most extreme velocities and in the velocity map of figure 9.

The NW turnover as described by Reakes and Newton (1978) is observed in detail in our data set over a large number of channel maps (-322.7 through -273.3 km s^{-1}). A somewhat identical feature, less prominent partly due to the primary beam attenuation and not observed by Reakes and Newton can be seen at the low velocity side as a SE extension (at -75.9 km s^{-1}), matching up with the NW turnover to form an outer disk with position angle $\sim -18°$.

5.2 ANOMALOUS VELOCITIES. — While reducing the WSRT data set we noticed an anomalous feature in the southern hemisphere of M33. The channel map showing this structure at highest intensity is the one at velocity -199.4 km s^{-1}. It can be followed over a range in velocity spanning some 56 km s^{-1}. At the time of writing it is unclear why such velocities can be present at one position, but the low surface brightness, enormous extent, and the forbidden velocity of this feature hint to a warp origin.

Other anomalous velocities can be found at the position of all spiral arms, as described by Humphreys and Sandage (1980). Deviations from circular motion of 10-40 km s^{-1} can be found at the crossing of spiral arms in the position-velocity maps along the major axis. The velocity extent and position of these deviations both point to the presence of density waves (Courtes and Doubout-Crillon, 1971 ; Newton, 1980). We will comment on these anomalous motions in detail in our analysis.

5.3 FINE SCALE DISTRIBUTION. — The resolution of this survey is high, revealing HI structures as small as 40 pc diameter. Thus a wealth of detail can be seen in the individual channel maps of figure 5. Although a television screen is the best way of displaying data with such a large dynamic range and high resolution, one can see many filaments, arcs, shell — and cloud — like structures, and regions which are devoid of emission in the channel maps as well as in the column density map of figure 8. We have underway in Leiden detailed studies of correlation between these fine scale structures in the neutral hydrogen distribution and OB associations, HII regions, SN remnants, and dust distribution.

Acknowledgements.

The WSRT is operated by the Netherlands Foundation for Radio Astronomy with the financial support of the Netherlands Organization for Advancement of Pure Research (Z.W.O.). As is described in this work short spacing data is of vital importance to a project of this kind. We are grateful to Dr. W. K. H. Huchtmeier, for putting his Effelsberg HI data at our disposal, and for reobserving a considerable part of an earlier survey. We thank R. Braun and R. A. M. Walterbos for their contribution to the problem of the short spacing baselines. We also benefited greatly from the help of E. Brinks. The many reproductions of the radio photographs were made by Mr. W. Brokaar, the Leiden Observatory photographer.

Appendix A.

A technique for restoring large-scale structure in synthesis maps has been described by Braun and Walterbos (1985). Their analytic expression for the Fourier transform of the 0- and 18-meter baselines of the WSRT u-v coverage enables us to extrapolate the missed data in a full synthesis. Because the M33 HI data available from the Effelsberg 100-m telescope covers only about half of the total HI extent of the galaxy, we made use of the Fourier fitting technique. Fourier fitting involves extrapolating the short-spacing information from the existing data to create a flat map plane, under the assumption that we know the fitting area to be free of emission in order to correct the negative zero level around extended emission regions. If the short-spacing visibilities are to be estimated accurately, the extended emission should cover less than 30′ or 75 % of the first grating ring radius. This is in fact only the case for the more extreme velocity maps, where the emission is clumped in small regions, because of the rotation characteristics of the galaxy (see Fig. 5). In our case the boundary was set by the dimensions of the fully-sampled Effelsberg HI data. If more than 10 % of the emission in the WSRT maps occurred outside that region we used the Braun-Walterbos technique.

We applied the Braun-Walterbos technique to some channels for which the short-spacing data were in fact available, in order to compare the results of the technique with the situation actually observed, and thus to test the accuracy of the Braun-Walterbos technique. The tests were performed on two channels symmetrically displaced from the systemic velocity. Those channel maps are at -211.8 and -125.3 km s^{-1}. Figure 3 shows that the extended emission covers more than 40′ right ascension ; therefore the Braun-Walterbos technique cannot fully restore the missing short-spacing information in this case. Because we have no correct Effelsberg data for channel maps were we know the Braun-Walterbos method to work better, this is the best we can do. We have smoothed the maps to eigth times the original resolution. The coordinate system has the declination compressed by a factor of two in order to give a circular beam in these maps. The broken contours indicate the outer boundary of the region fit and the box contours indicate the fully-sampled Effelsberg area. Vertical cross-cuts through these maps are shown below each panel. It is clear from the cross-cut plots that the Braun-Walterbos technique is not capable of retrieving all

emission, but up to 90 % has been restored. There is still a hint for a central depression, but this is only a small effect compared to the original bowl. The multi-resolution clean used by Brinks (1984) is another technique for extrapolating short-spacing information from the existing WSRT data. This technique, however, is in our case only capable of retrieving 75 % of the missed short-spacing data. The high-velocity channel map gives rise to the largest difference, because of its large extended emission. We know from earlier HI surveys (e.g. Rogstad *et al.*, 1976) that M33 shows double profiles indicative of a warped hydrogen layer. Such an HI distribution would give rise to low brightness large extended emission that could not be retrieved by the Braun-Walterbos technique, because that technique requires a large area free from emission. The cross-cuts of figure 3(c) and (d) show such low brightness, large extended emission that, under the assumptions of the Braun-Walterbos technique can never be retrieved.

Another way of judging the accuracy of the Braun-Walterbos technique involves to look for emission discontinuities between lines of equal velocity in position-velocity maps along the major axis. If we take the major axis profile of the present version, with the smoothing as described in section 3.1, we can still see (Fig. 6) that the Braun-Walterbos technique has restored most of the missing short-spacing emission, but as indicated above, especially at the low velocity side a discontinuity of the order of a few percent is still present (near -125 km s^{-1}).

References

BAARS, J. W. M., HOOGHOUDT, B. G. : 1974, *Astron. Astrophys.* **31,** 323.
BAJAJA, E., ALBADA, G. D. VAN : 1979, *Astron. Astrophys. Suppl. Ser.* **49,** 745.
BOS, A., RAIMOND, E., SOMEREN GREVE, H. W. VAN : 1981, *Astron. Astrophys.* **98,** 251.
BOSMA, A. : 1981, *Astron. J.* **86,** 1825.
BRAUN, R., WALTERBOS, R. A. M. : 1985, *Astron. Astrophys.* **143,** 307.
BRINKS, E. : 1984, *Astron. Astrophys. Suppl. Ser.* **55,** 179.
BRINKS, E., BURTON, W. B. : 1984, *Astron. Astrophys.* **141,** 195.
BROUW, W. N. : 1975, in *Methods in Computational Physics,* Eds. B. Alder, S. Fernbacher and M. Rotenberg (Academic Press) **14,** 131.
BURKE, B. F., TURNER, K. C., TUVE, M. A. : 1963, *Carnegie Inst. Washington Year Book 1962,* p. 289.
CASSE, J. C., MULLER, C. A. : 1974, *Astron. Astrophys.* **31,** 333.
COURTÈS, G., DUBOUT-CRILLON, R. : 1971, *Astron. Astrophys.* **11,** 468.
DIETER, N. H. : 1962, *Astron. J.* **67,** 217.
GORDON, K. J. : 1971, *Astrophys. J.* **169,** 235.
HARTEN, R. H. : 1974, in Netherlands Foundation of Radio Astronomy, *Int. Techn. Rep.* **121** (rev. 1975).
HERZOG, A. D., ILLINGWORTH, G. : 1977, *Astrophys. J. Suppl. Ser.* **33,** 55.
HÖGBOM, J. A. : 1974, *Astron. Astrophys. Suppl. Ser.* **15,** 417.
HÖGBOM, J. A., BROUW, W. N. : 1974, *Astron. Astrophys.* **33,** 289.
HOLMBERG, E. : 1950, *Lunds Obs. Medd. Ser. II No.* **128.**
HUCHTMEIER, W. : 1972, *Astron. Astrophys. Suppl. Ser.* **7,** 397.
HUCHTMEIER, W. : 1973, *Astron. Astrophys.* **22,** 91.
HUCHTMEIER, W. : 1977, private communication.
HUMPHREYS, R. M., SANDAGE, A. : 1980, *Astrophys. J. Suppl. Ser.* **44,** 319.
JAGER, G. de, DAVIES, R. D. : 1971, *Mon. Not. R. Astron. Soc.* **153,** 9.
MADORE, B. F., MCALARY, C. W., MCLAREN, R. A., WELCH, D. C., NEUGEBAUER, G., MATTHEWS, K. : 1985, *Astrophys. J.* **294,** 560.
MENG, S. Y., KRAUS, J. D. : 1966, *Astron. J.* **71,** 170.
NEWTON, K. : 1980, *Mon. Not. R. Astron. Soc.* **190,** 689.
REAKES, M. L., NEWTON, K. : 1978, *Mon. Not. R. Astron. Soc.* **185,** 277.
ROGSTAD, D. H., WRIGHT, M. C. H., LOCKHART, I. A. : 1976, *Astrophys. J.* **204,** 703.
SANDAGE, A., TAMMANN, G. A. : 1981, *A revised Shapley-Ames Catalog,* Carnegie Institution of Washington Pub. No. **635.**
SCHWARZ, U. J. : 1978, *Astron. Astrophys.* **65,** 345.
SOMEREN GREVE, H. W. VAN : 1974, *Astron. Astrophys. Suppl. Ser.* **15,** 343.
VAUCOULEURS, G., LEACH, R. W. : 1981, *Publ. Astron. Soc. Pac.* **93,** 190.
VOLDERS, L. M. J. S. : 1959, *Bull. Astron. Inst. Neth.* **14,** 323.
WEVERS, B. M. H. R. : 1984, Ph. D. thesis, University of Groningen (The Netherlands).
WRIGHT, M. C. H., WARNER, P. J., BALDWIN, J. E. : 1972, *Mon. Not. R. Astron. Soc.* **155,** 337.

TABLE I. — *General information on M33.*

Morphological Type	Scd II - III	Sandage and Tammann	(1981)
Distance	724 +/- 70 kpc 12" ==> 42 pc	Madore et. al	(1985)
Position of nucleus	Ra (1950) $1^h31^m01^s.57$ Dec(1950) 30°24'15".0 l (1950) 133°.69 b (1950) -31°.35	De Vaucouleurs and Leach	(1981)
PA of Major axis	22° ±4	This paper	
Inclination angle	57° ±6	This paper	
Holmberg Diameter Radius	83' x 53' 8.7 kpc	Holmberg	(1975)
HI Radius Disk Extensions	7 kpc 14 kpc	Newton	(1980)
Systemic Velocity	-181.0 ±1.3 km s^{-1}	This paper	

TABLE II. — *Surveys of the 21-cm line in M33.*

Observers	Telescope	Angular Resolution (')	Vel. Res. Km/s	Extent Ra x Dec (min x ')
Volders (1959)	Dwingeloo 25m	34	33	9 x 120
Dieter (1962)	Harvard 18m	53	17	30 x 150
Burke et al.(1963)	Green Bank 90m	10.0	2.1	maj. + min axis
Meng and Kraus (1966)	Ohio State 80m/24m	10 x 38	100	
de Jager,Davies (1971)	Jodrell Bank 75m	14 x 18	8.4	20 x 132
Gordon (1971)	Green Bank 90m	10.0 x 11.4	21	30 x 135
Wright et al.(1972)	Cambridge 2 x 12m	1.5 x 3.0	39	12 x 120
Huchtmeier (1972)	Nancay 40 x 200m	4 x 24	12.7	16.5 x 120
Rogstad et al.(1976)	Owens Valley 2 x 27.4m	2	10	12 x 48
Huchtmeier (1977)	Effelsberg 100m	12	6.5	180 x 162
Reakes and Newton(1978)	Cambridge Half Mile 12 x 12 x 12m	7 x 15	16	8 x 165
Newton (1980)	Cambridge Half Mile 60 x 12 x 12m	1.5 x 3.0	16	12 x 93
Deul and van der Hulst (this paper)	Westerbork (WSRT) 40 x 12 x 25m	0.2 x 0.4	8.2	6 x 105

TABLE III. — *Observational parameters of the Westerbork M33 Survey.*

Field	SE	NW
Fringe Stopping Center Ra (1950)	$1^h\ 30^m\ 49^s$	$1^h\ 32^m\ 30^s$
Dec(1950)	$30^o\ 17'\ 23''$	$30^o\ 38'\ 00''$
Heliocentric velocity of passband center	-150.0 km s^{-1}	-232.2 km s^{-1}
Number of channels	64	64
Number of baselines	156	160
Baselines in meters	36 (18) 2772	36 (18) 2772
R.M.S. noise at map center	2.8 mJy 6.7 K	2.1 mJy 5.0 K
Fraction of missed baselines	5.2 %	2.1 %
Observing dates in ddmmyy	220782,100882 070982,130982 170982,230982	270683,150783 160883,050983
Primary beam half power	19' x 37' (Ra x Dec)	
Mean synthesized beam half power	12" x 24" (Ra x Dec)	
System temperature	54 K	
Theoretical noise	1.45 mJy	
First grating ring diameter	40' x 79'	
Channel seperation	4.12 km s^{-1}	
Velocity resolution	8.24 km s^{-1}	
Frequency taper	Hanning	
UV Taper	Gaussian (0.25 at 2772m)	

TABLE IV. — *Calibration sources used in the M33 Survey.*

Calibrator	Ra (1950)	Dec (1950)	Flux
3C147	$05^h\ 38^m\ 43^s506$	49° 49' 42"83	21.57 Jy
3C286	$13^h\ 28^m\ 49^s654$	30° 45' 58"70	14.85 Jy
3C309.1	$14^h\ 58^m\ 56^s644$	71° 52' 11"5	7.84 Jy

TABLE V. — *Fluxes of point sources subtracted from the line data.*

Point sources subtracted		Ra (1950)	Dec (1950)	Flux density
Field	SE 1	$01^h\ 29^m\ 33^s7$	30° 28' 43"1	14.5 mJy/beam
Field	NW 1	$01^h\ 29^m\ 33^s7$	30° 28' 43"1	6.9 mJy/beam
	2	$01^h\ 31^m\ 39^s8$	30° 47' 48"6	6.6 mJy/beam

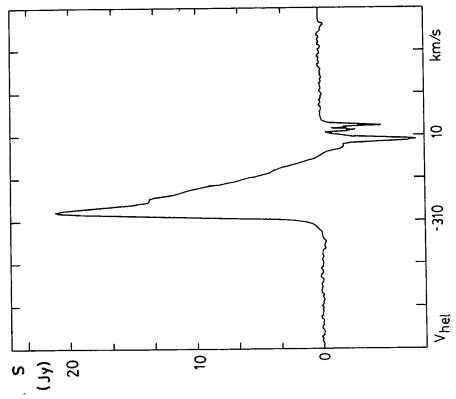

FIGURE 2. — HI emission profile observed with the Dwingeloo 25 m telescope at the Westerbork north-western fringe stopping center. M33 is seen in emission, but emission from the Milky Way appears in absorption because of the beam switching technique employed.

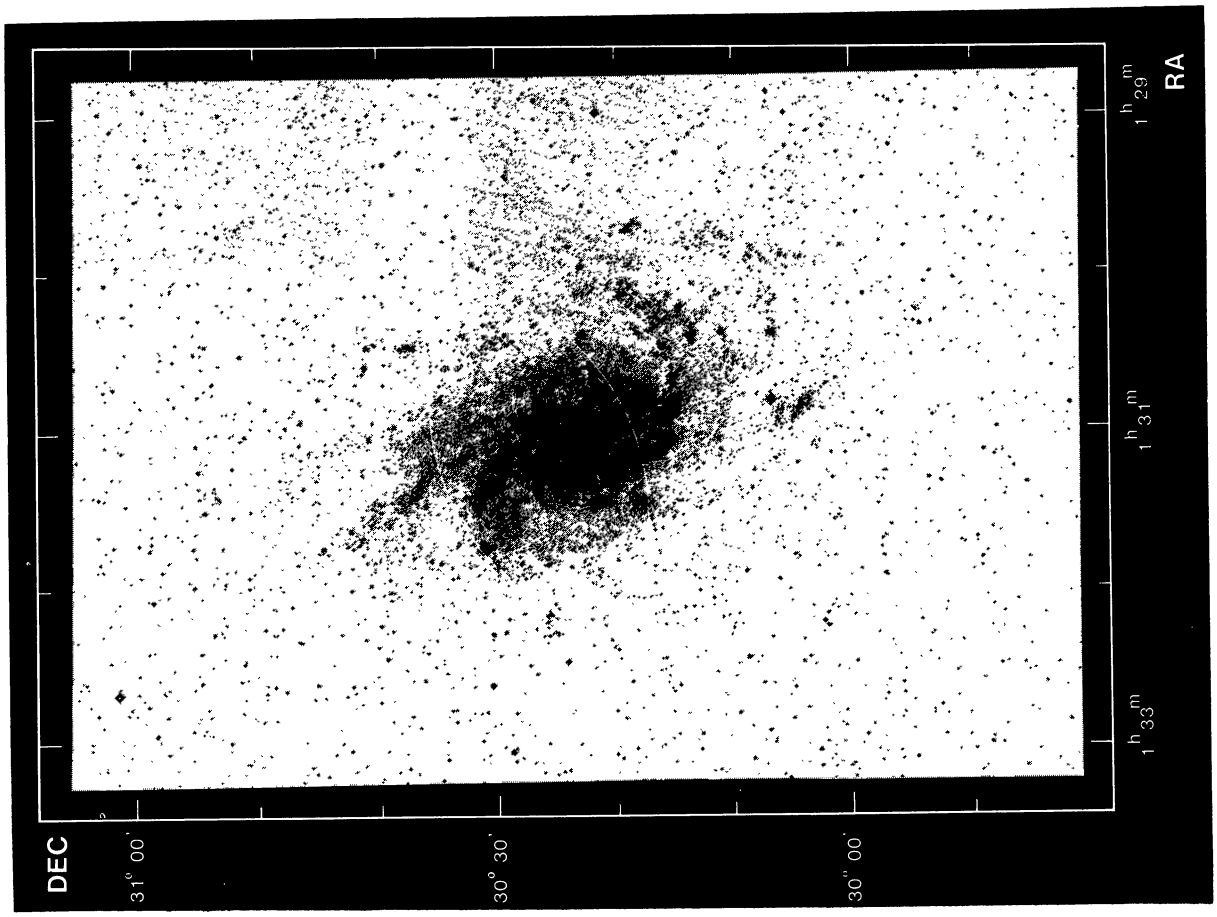

FIGURE 1. — Copy of the Palomar Sky Survey blue plate of M33 with contours of the half power circles of both Westerbork fields superimposed. The crosses indicate the corresponding fringe stopping centers.

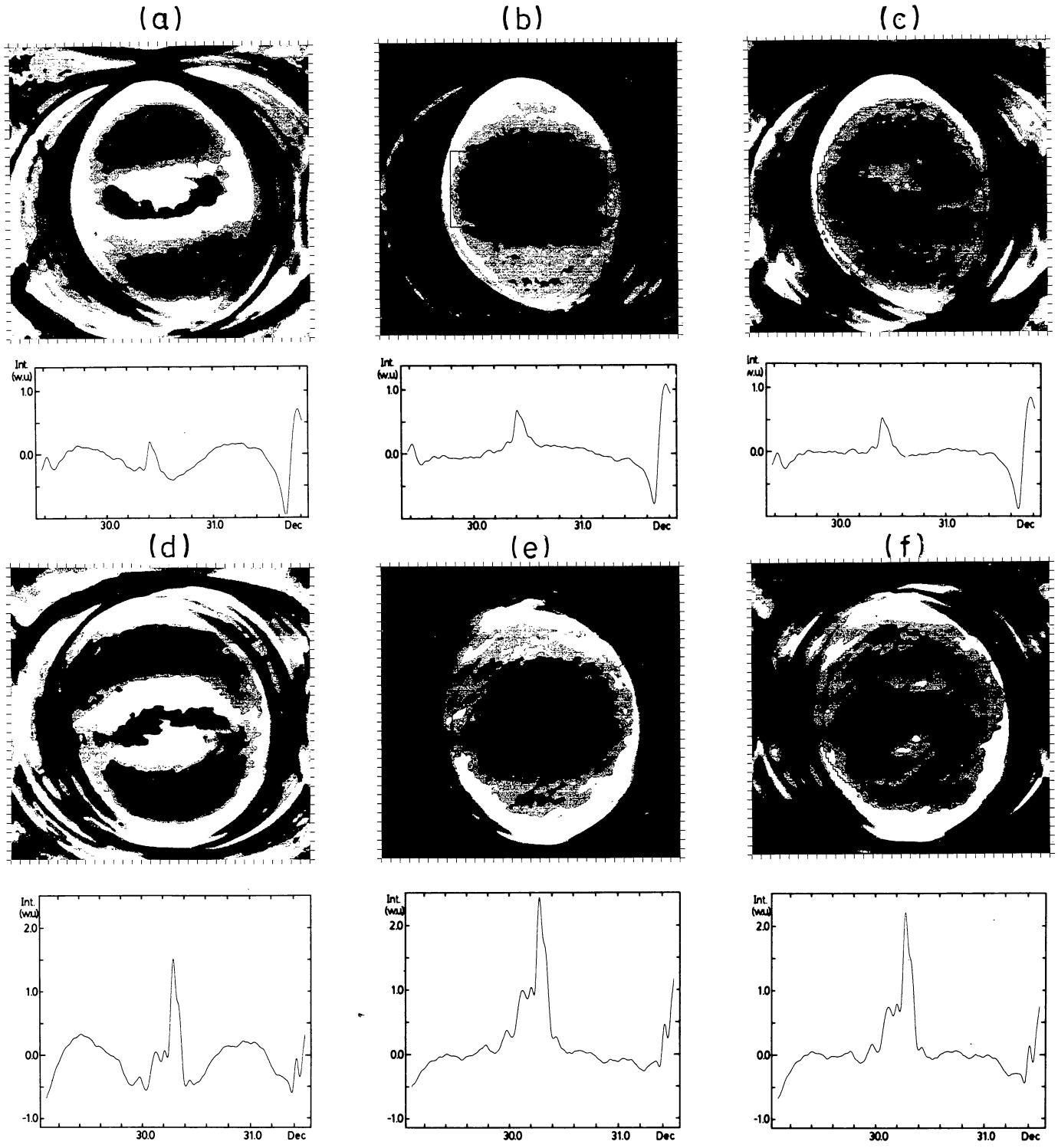

FIGURE 3. — Channel maps at – 125.3 km s^{-1} and – 211.8 km s^{-1} smoothed to eight times the original resolution. Vertical cross cuts through the map centers are shown below each map. Panels (a) and (d) : These maps only include the Westerbork data. Notice the « bowl » like feature in which the emission appears. Panels (b) and (e) : These maps include both the Westerbork and Effelsberg data. There is no trace of any « bowl » like feature, but there is a slide hint for large scale, low brightness emission. Panels (c) and (f) : These maps include the Westerbork data and are corrected using the Fourier fitting method. Only a slight hint of a « bowl » like feature can be seen in the crosscut plots.

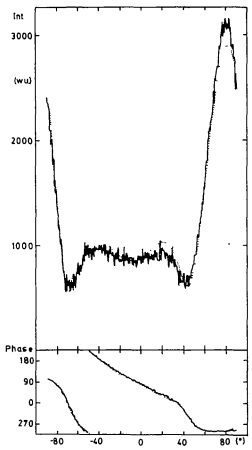

FIGURE 4. — The 36-meter data from the north western field. The full drawn line shows the measured Westerbork amplitude and phase angle, the dotted lines are the 36-meter amplitude and phase angles extracted from the Huchtmeier's Effelsberg data.

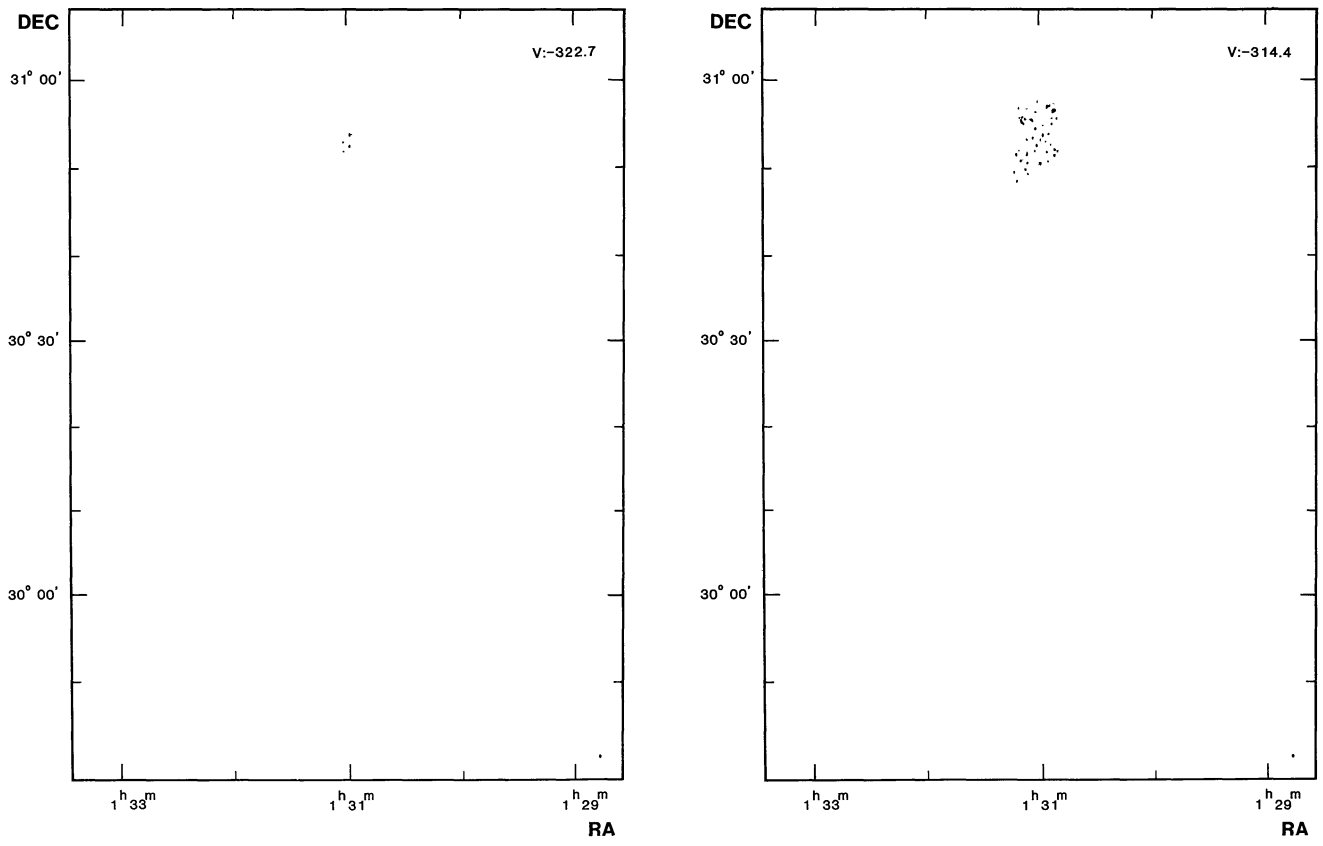

FIGURE 5. — Plots of the separate channel maps, at the individual velocities. The contours correspond to the full-resolution maps ; the grey scale corresponds to the data smoothed to 24″ × 48″ resolution. The contour levels are at 6.0, 13.2, 27.2, 37.3, 51.1, 70.1, and 96.0 K (T_b) and grey levels are at 1.2, 2, 5.4, 7.2, 13.2, 27.2, 37.3, 51.1 and 96.0 K (T_b).

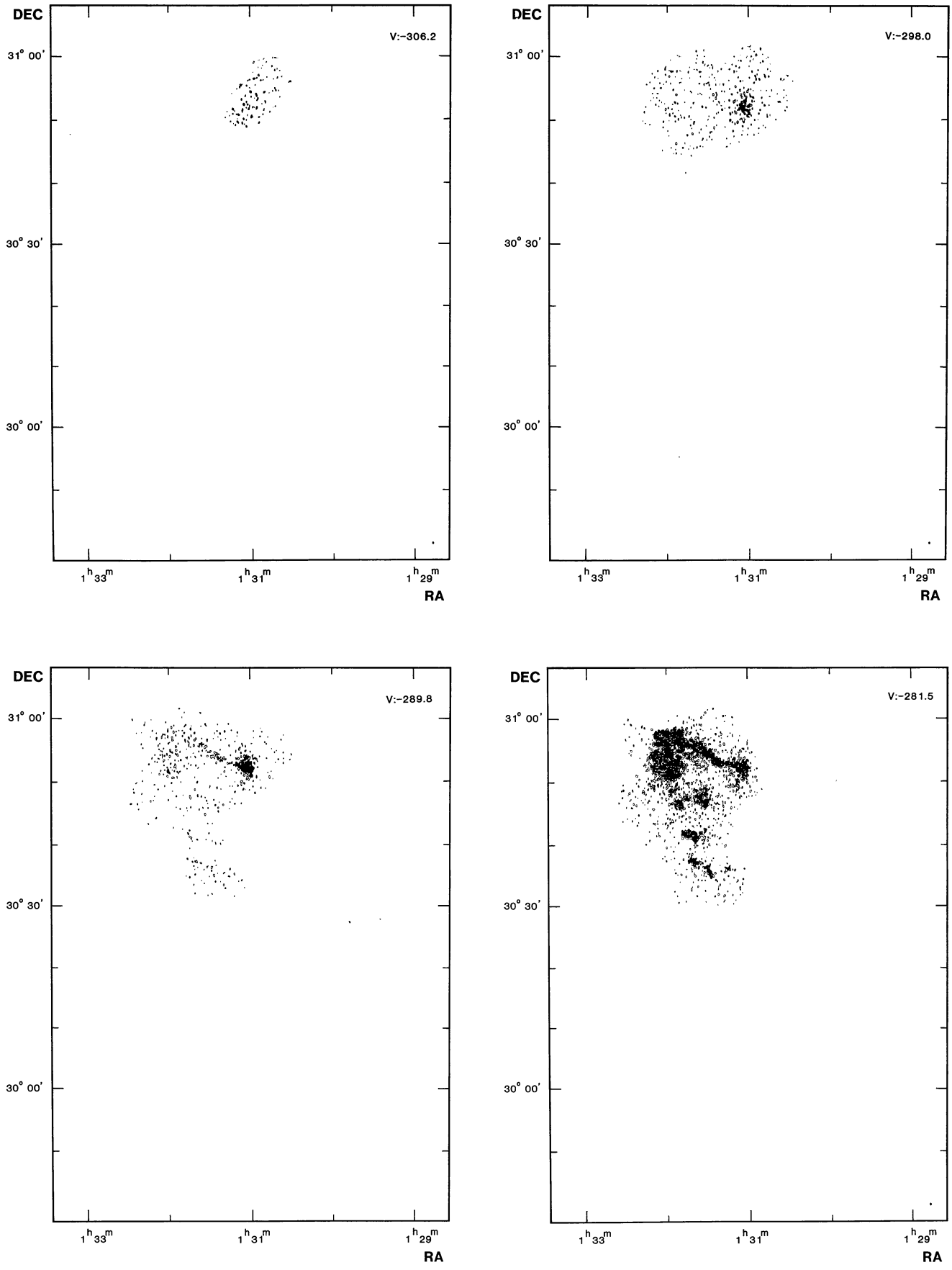

FIGURE 5 *(continued).*

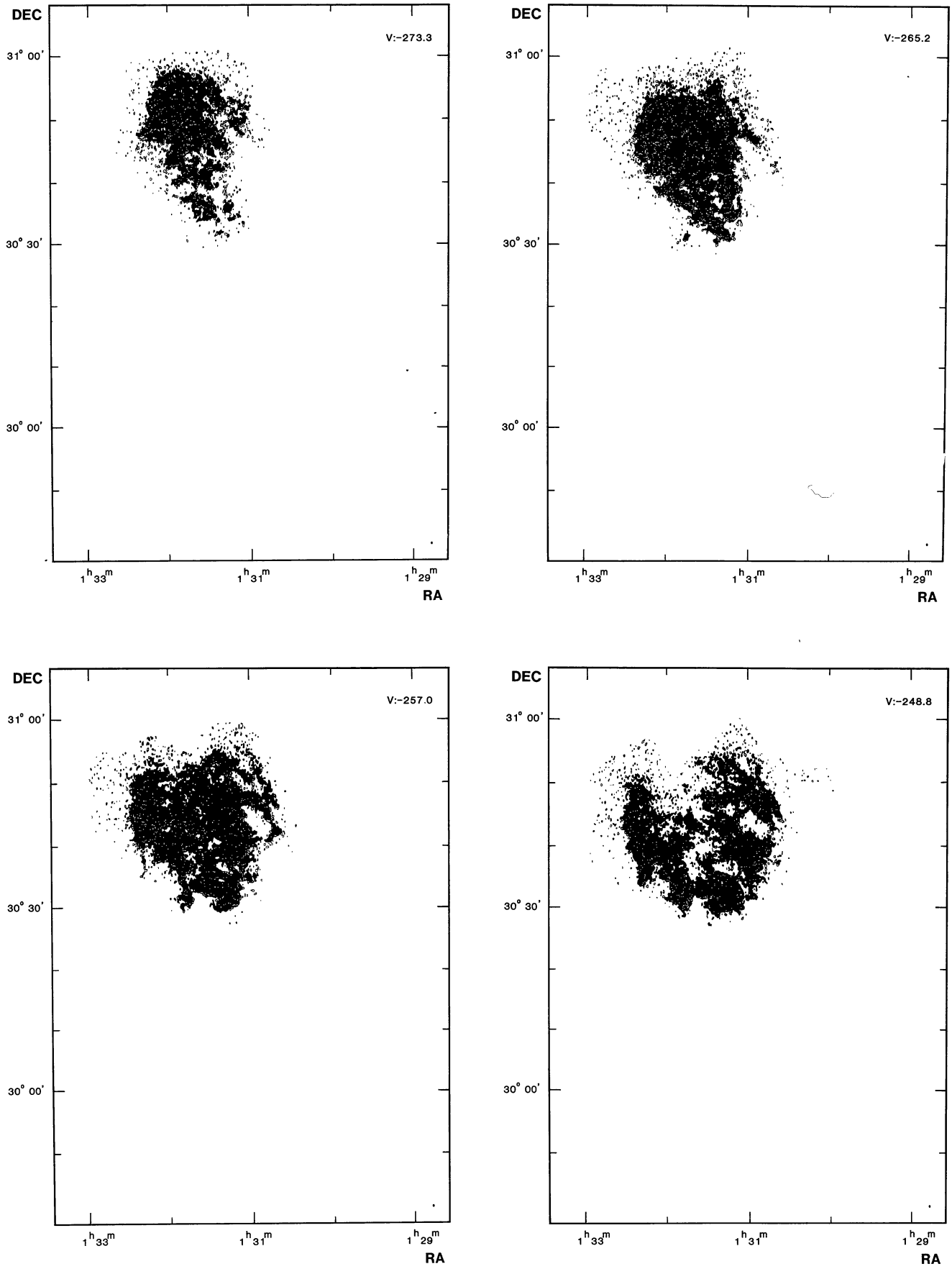

FIGURE 5 *(continued)*.

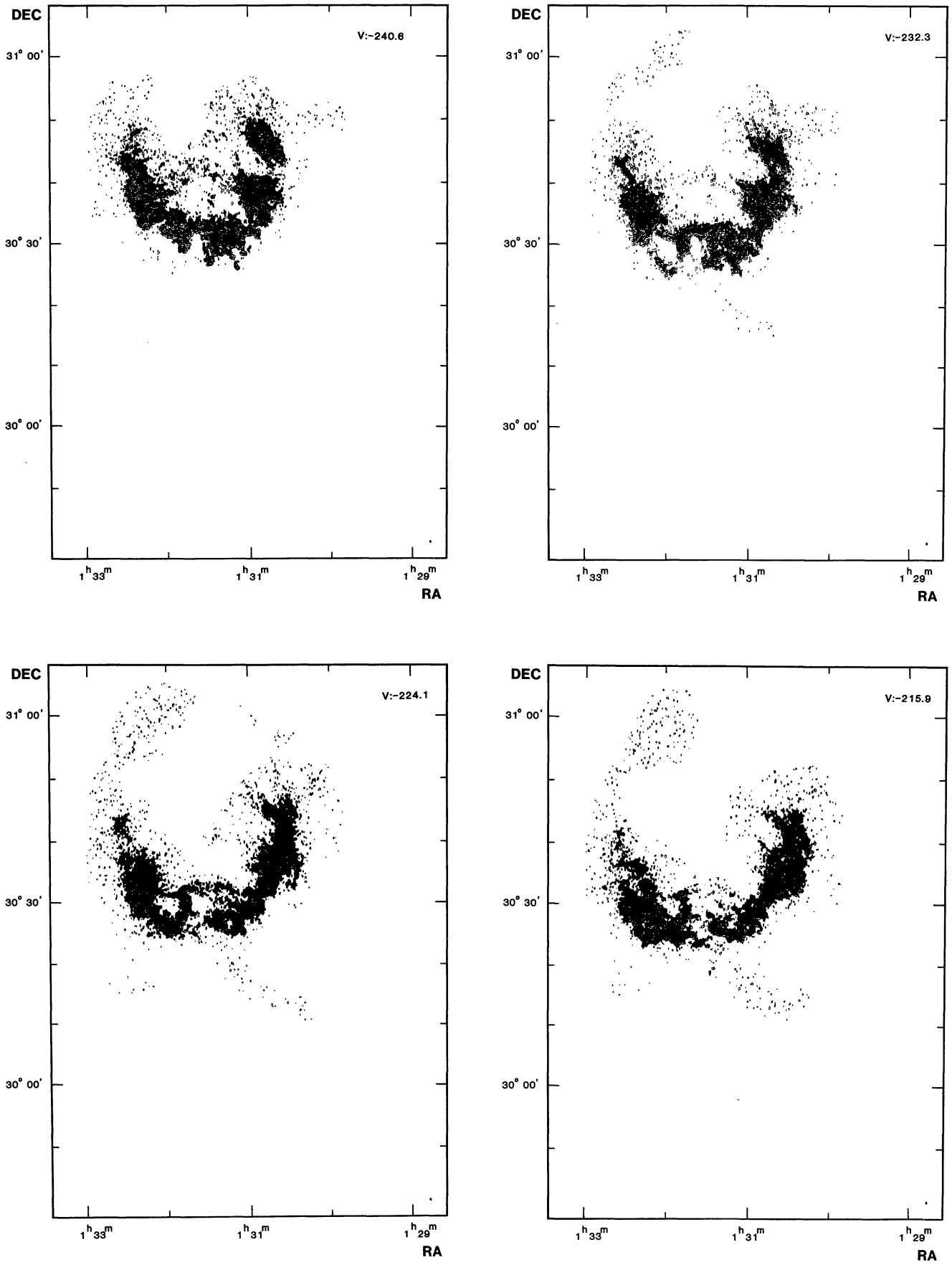

FIGURE 5 *(continued).*

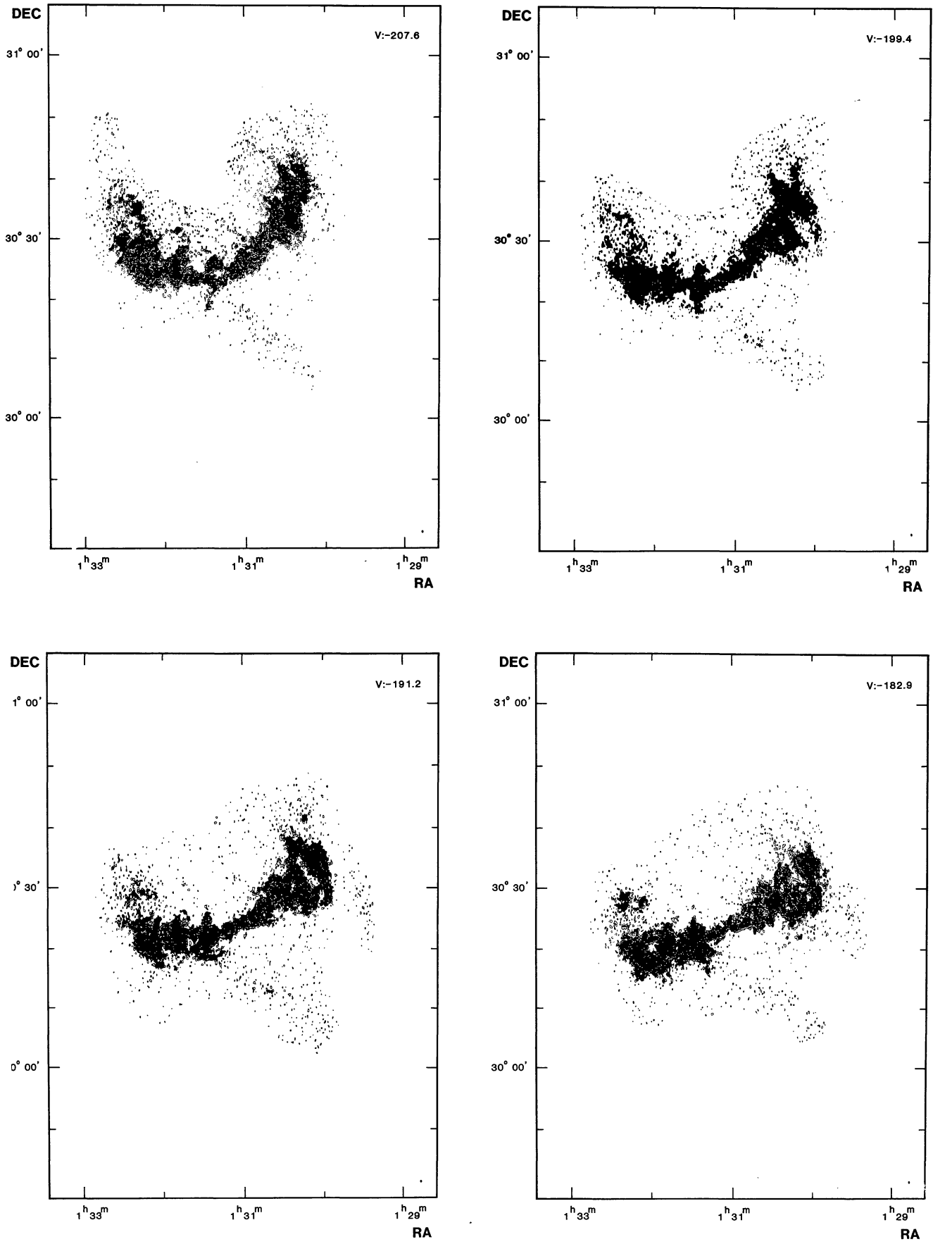

FIGURE 5 *(continued).*

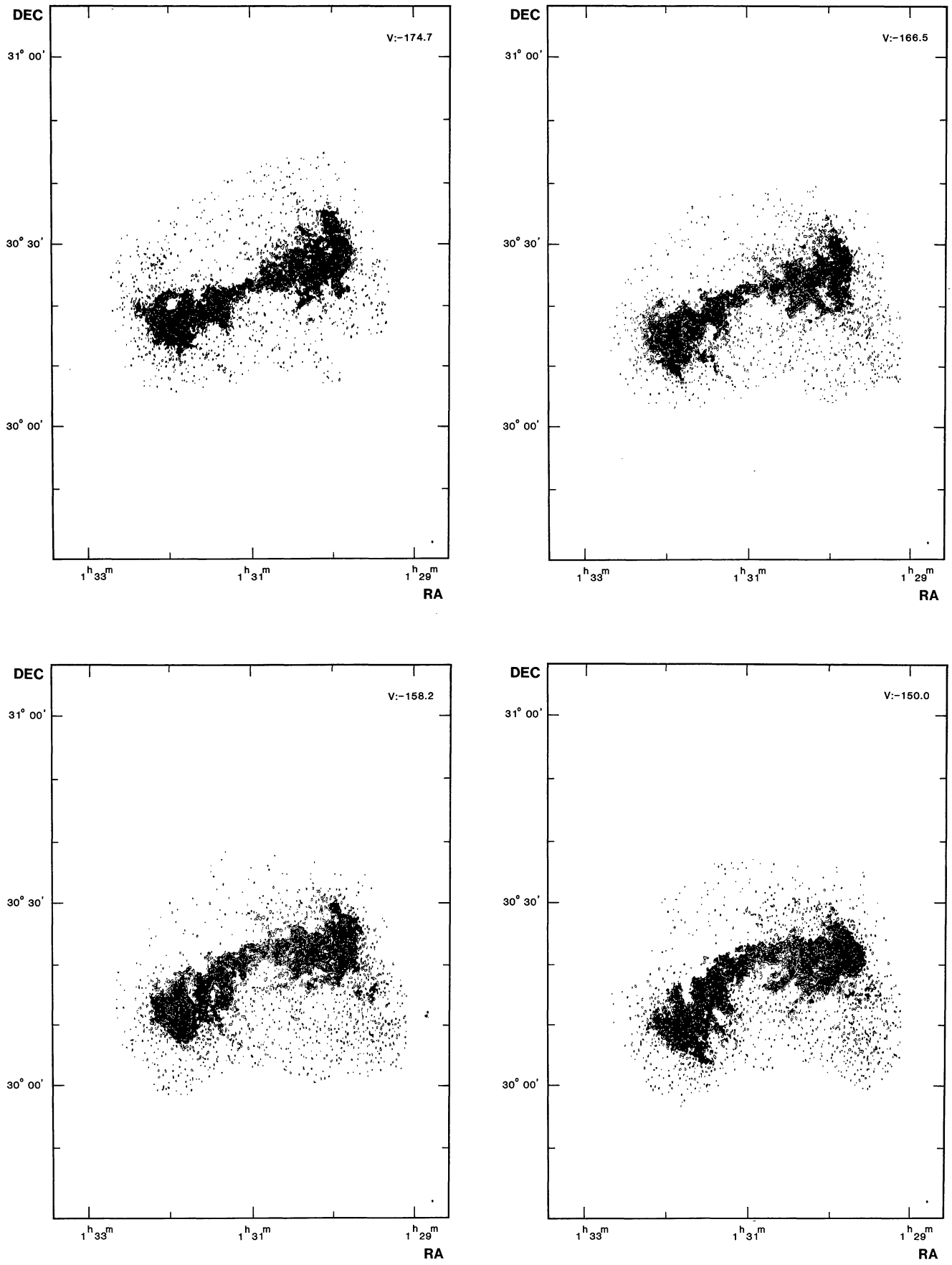

FIGURE 5 *(continued).*

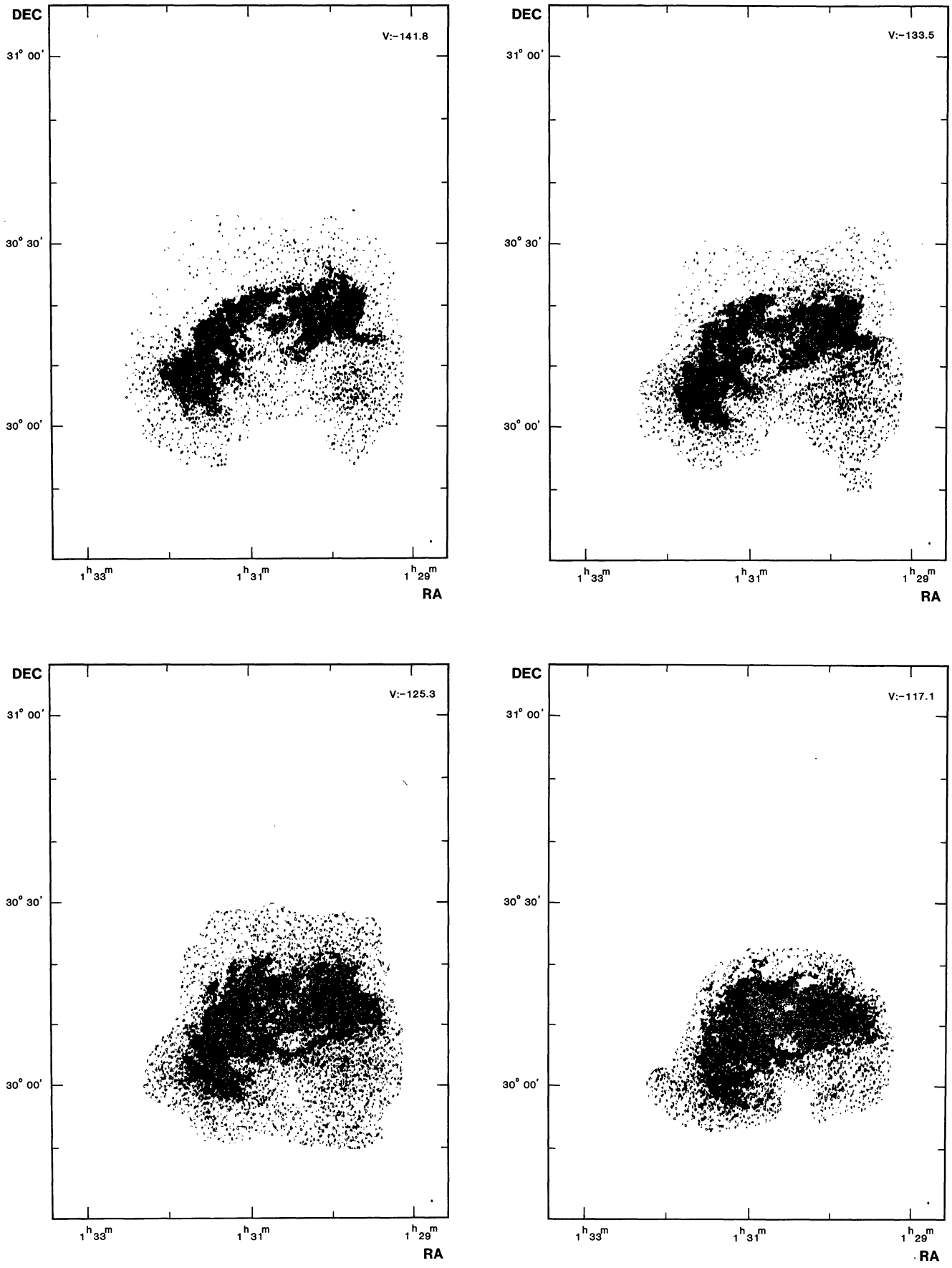

FIGURE 5 *(continued)*.

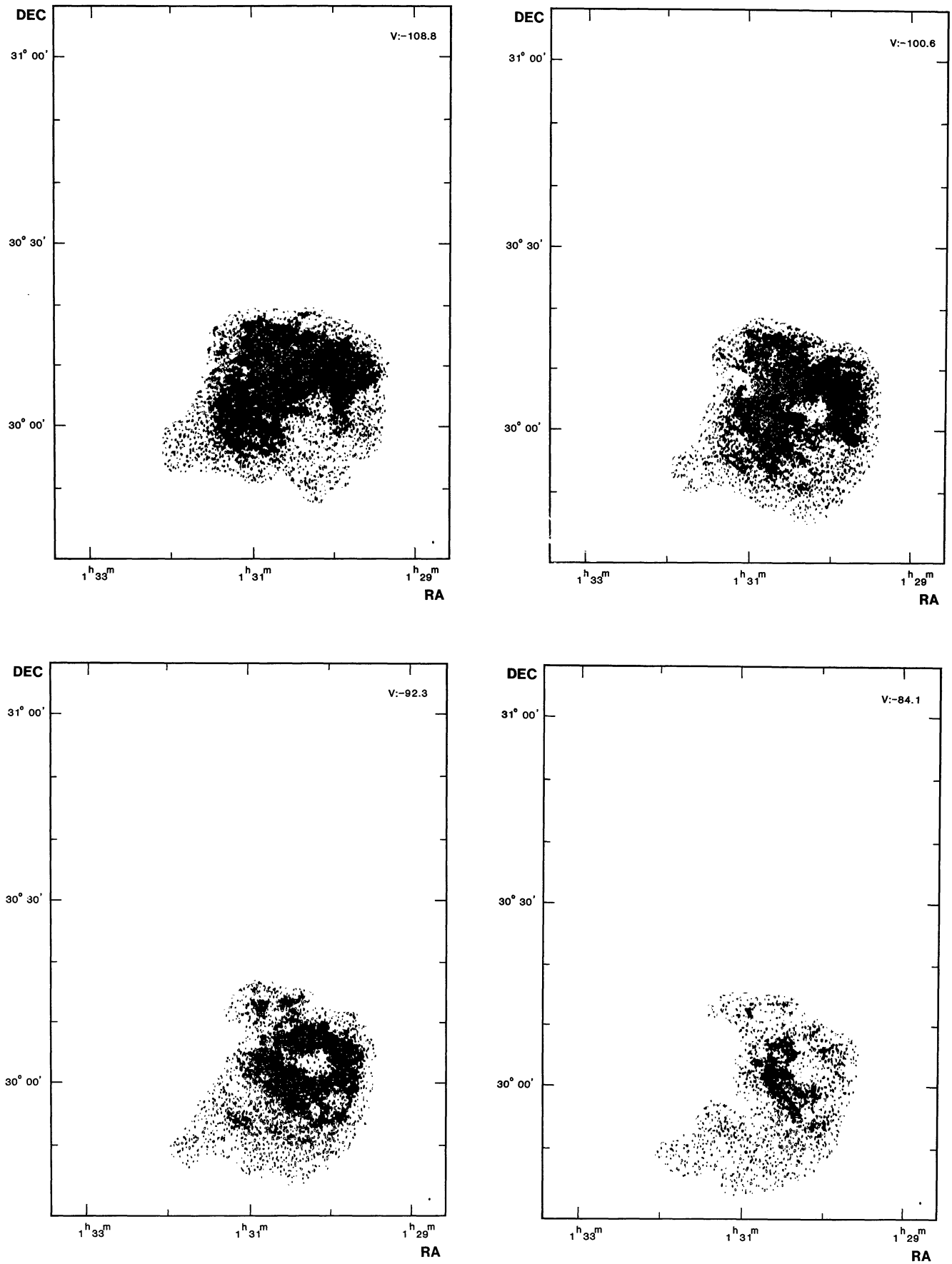

FIGURE 5 *(continued).*

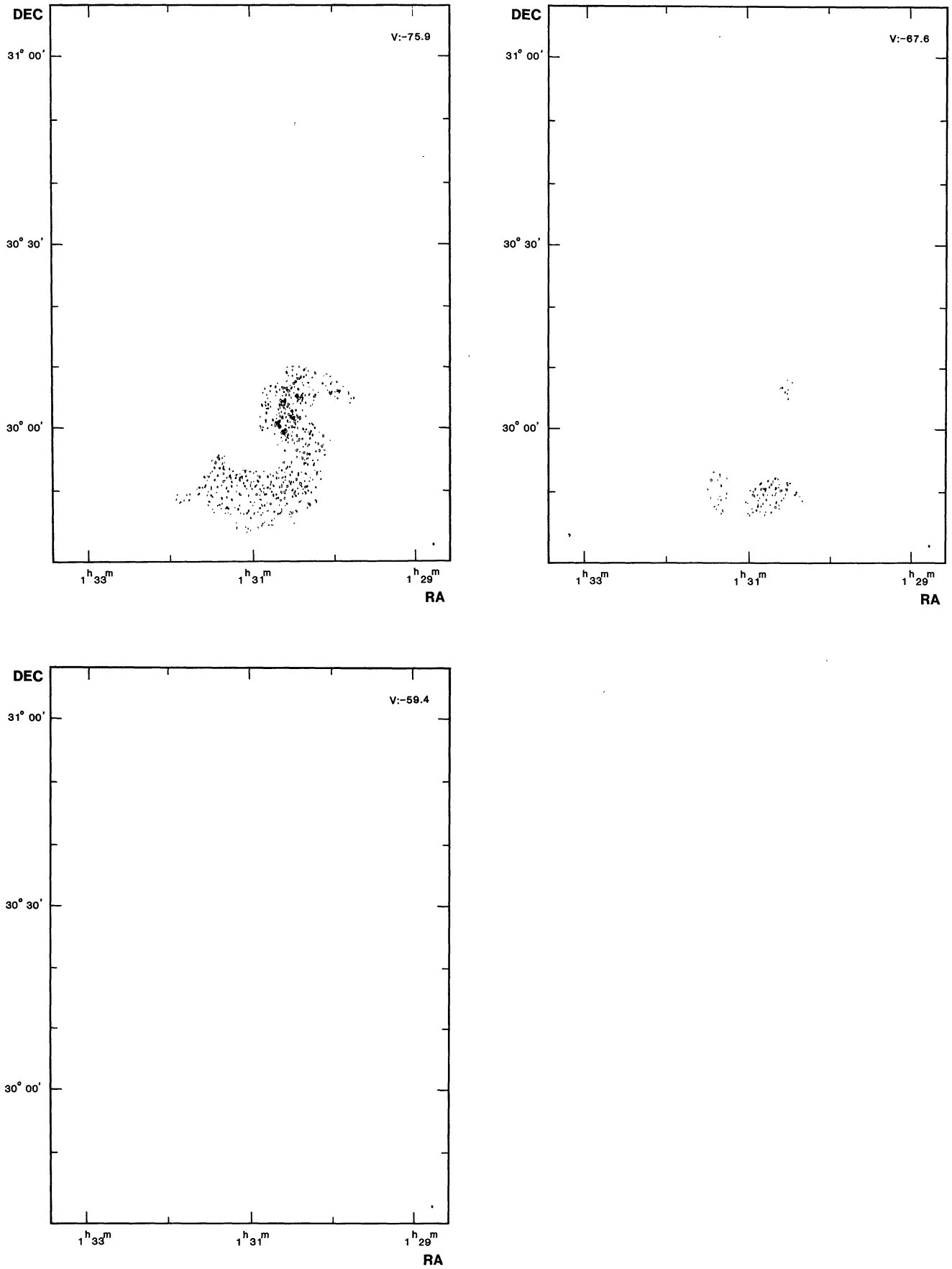

FIGURE 5 *(continued)*.

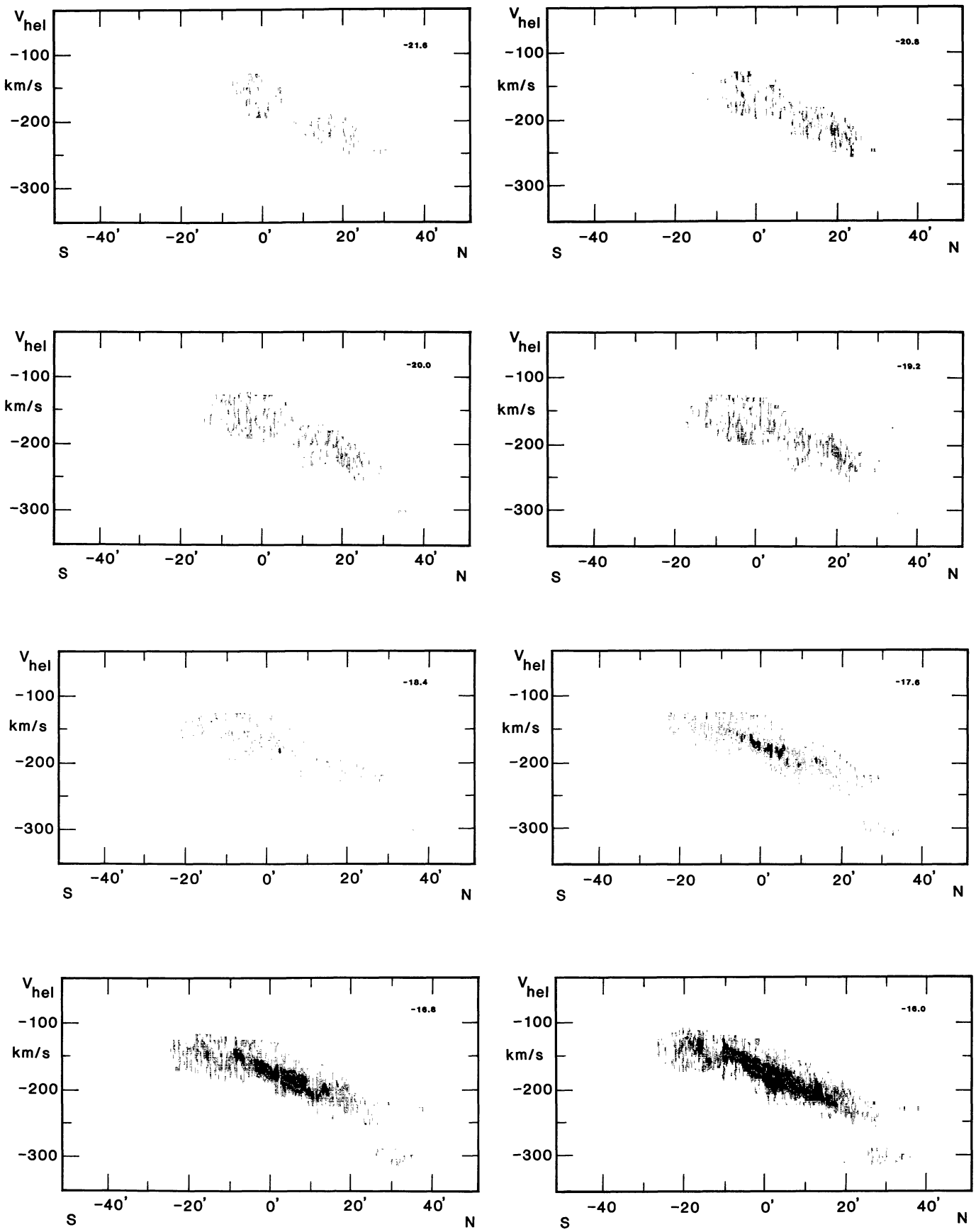

FIGURE 6. — Plots of position-velocity maps, along crosscuts parallel to the major axis of M33. The perpendicular distance from the major axis is indicated at the top righthand of each frame. The contours and grey levels are drawn at the values indicated in the caption to figure 5.

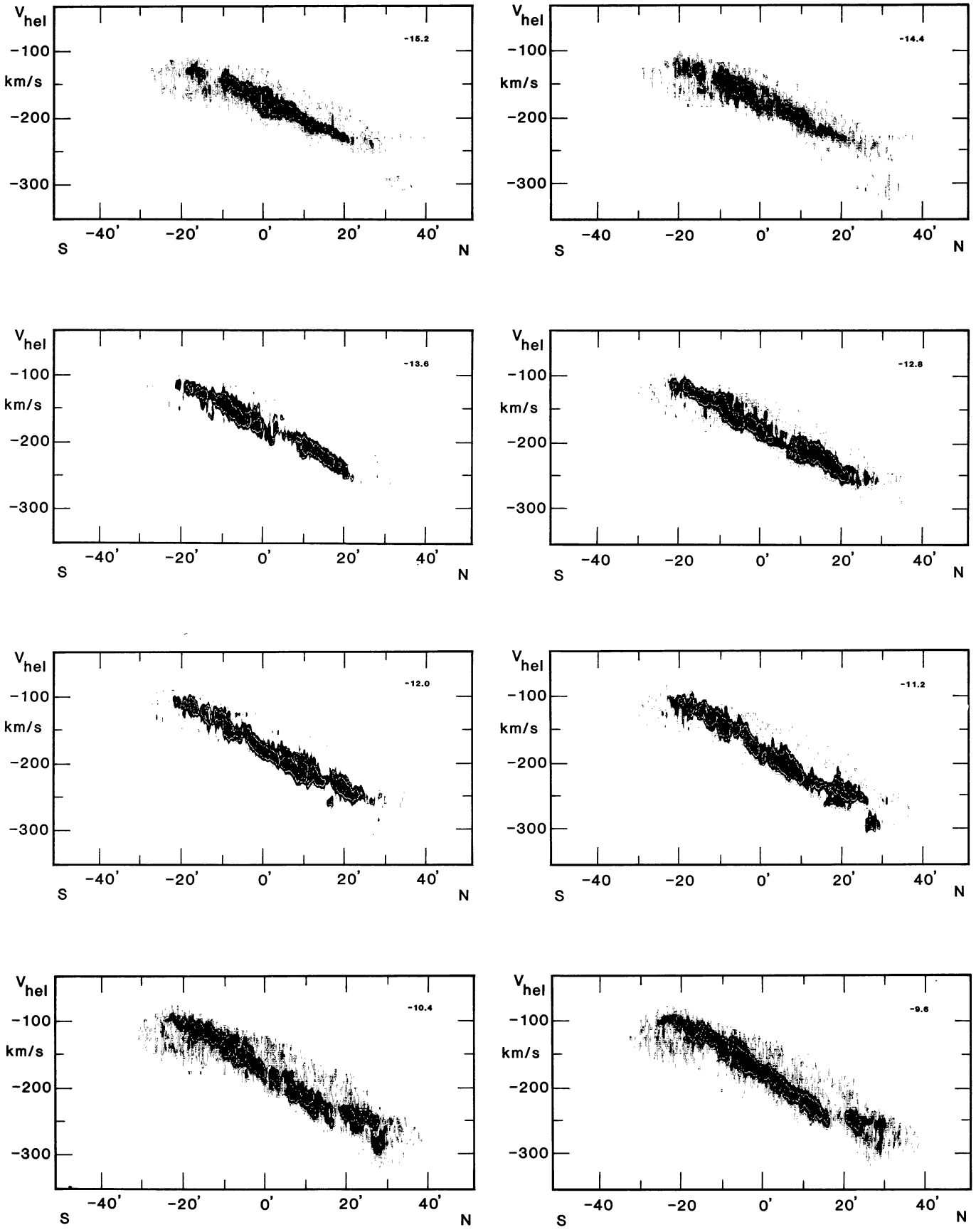

FIGURE 6 *(continued).*

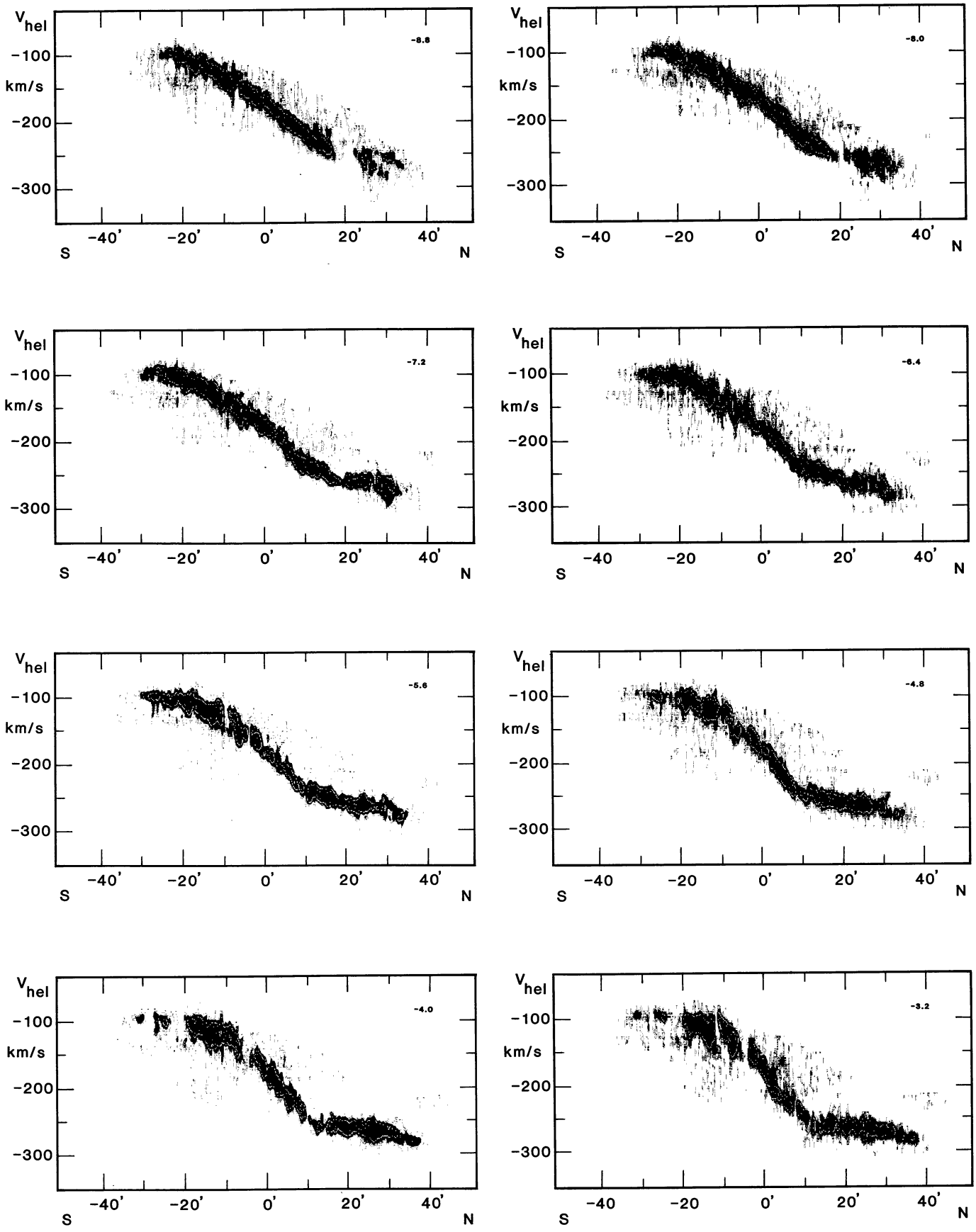

FIGURE 6 *(continued)*.

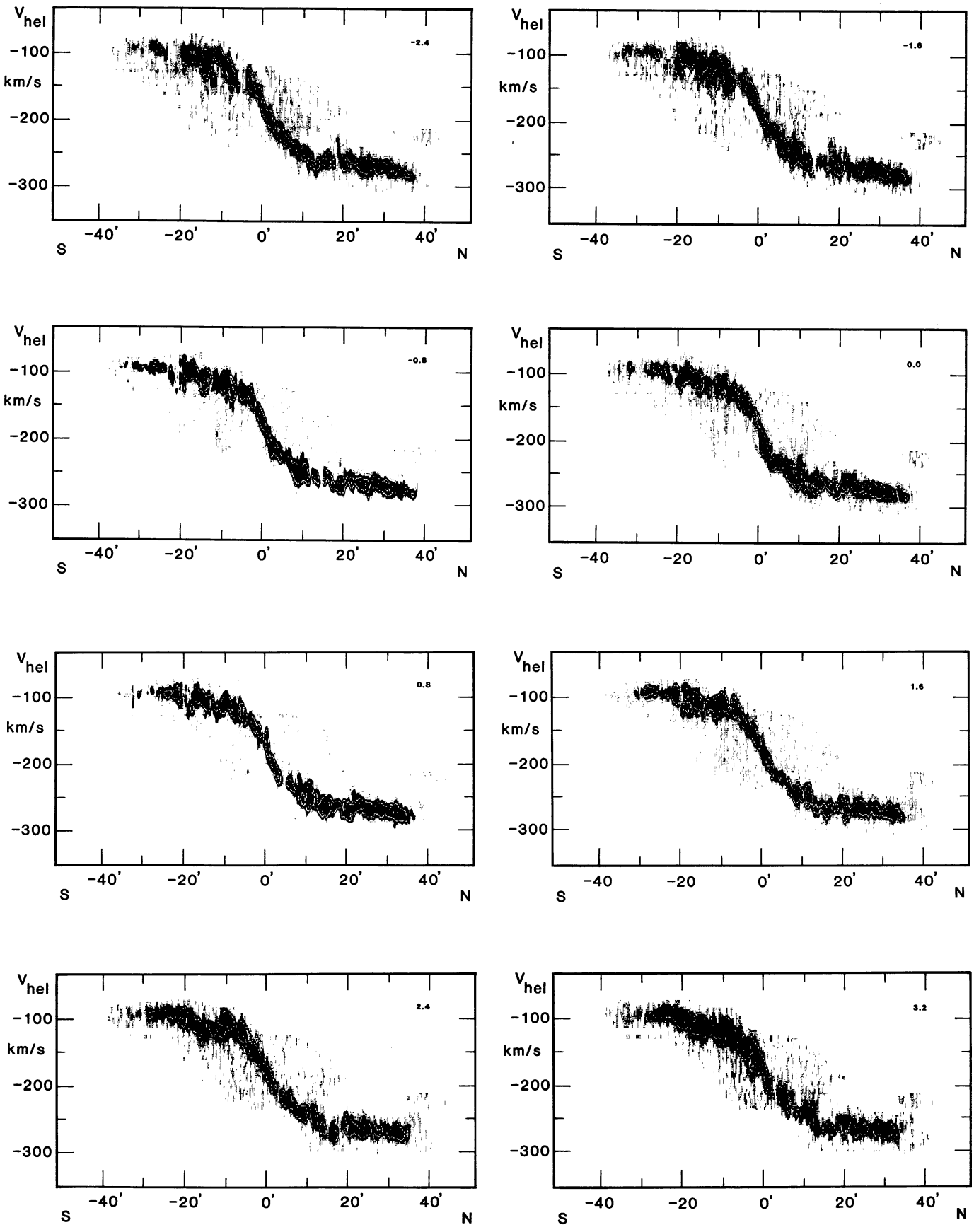

FIGURE 6 *(continued)*.

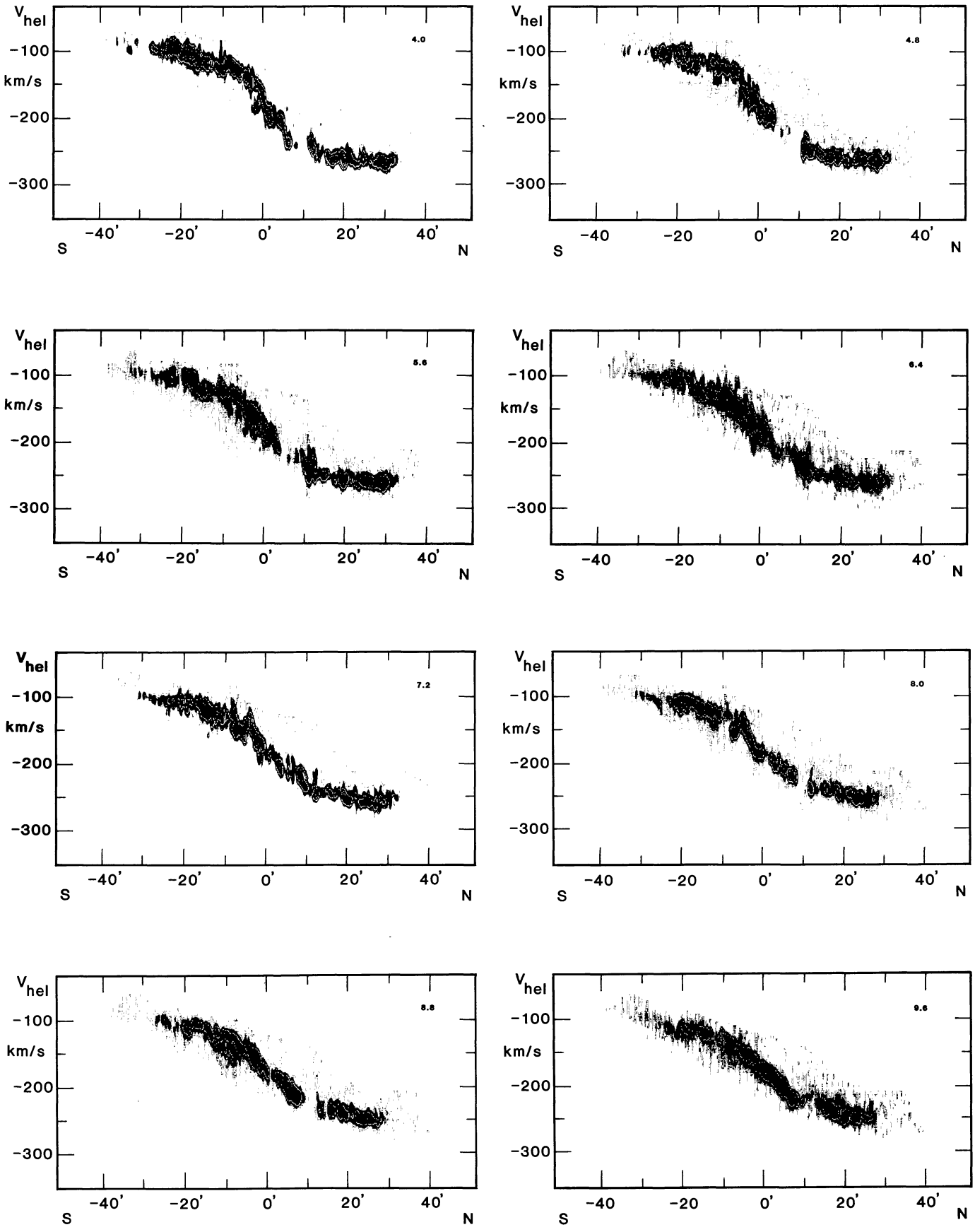

FIGURE 6 *(continued).*

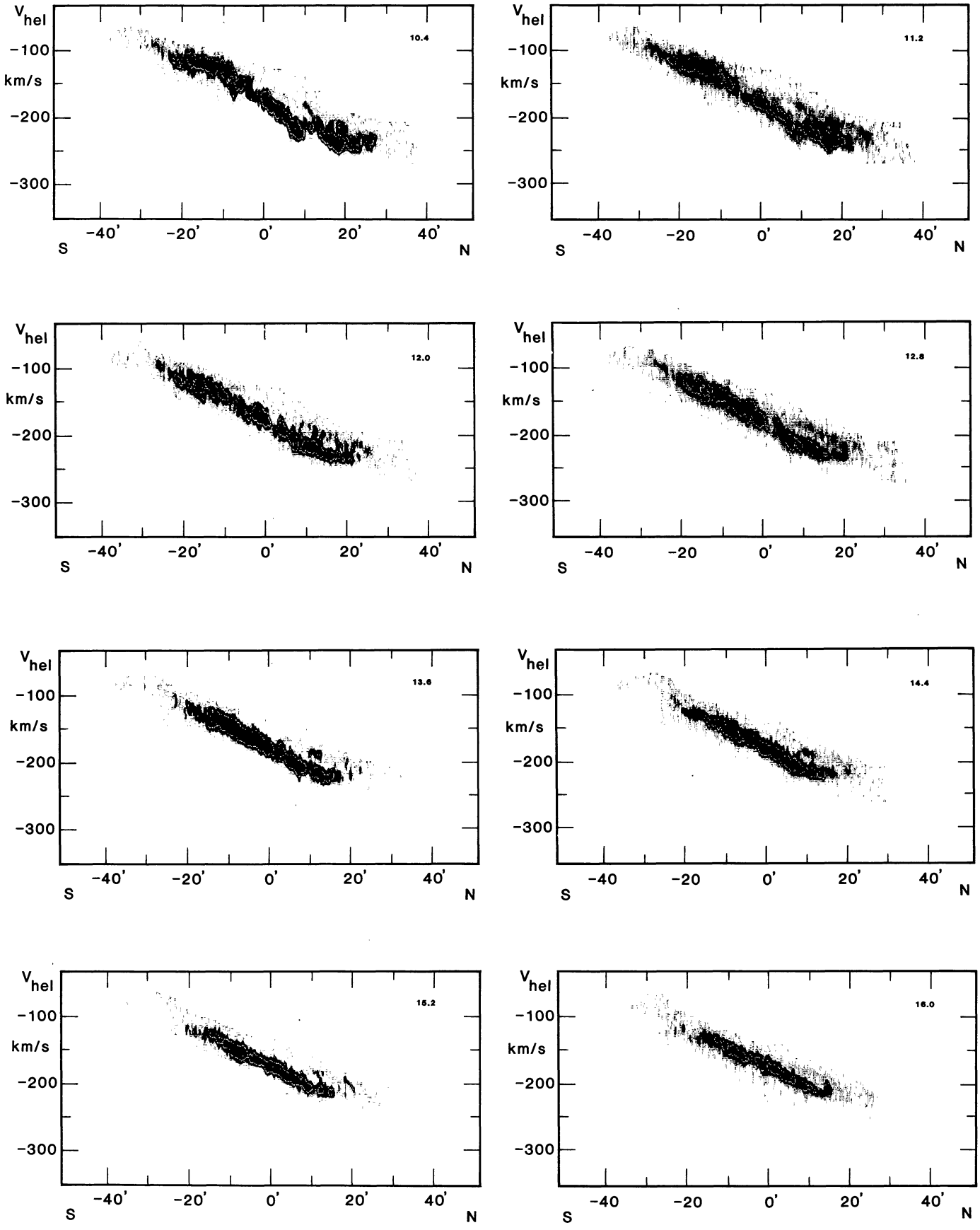

FIGURE 6 *(continued)*.

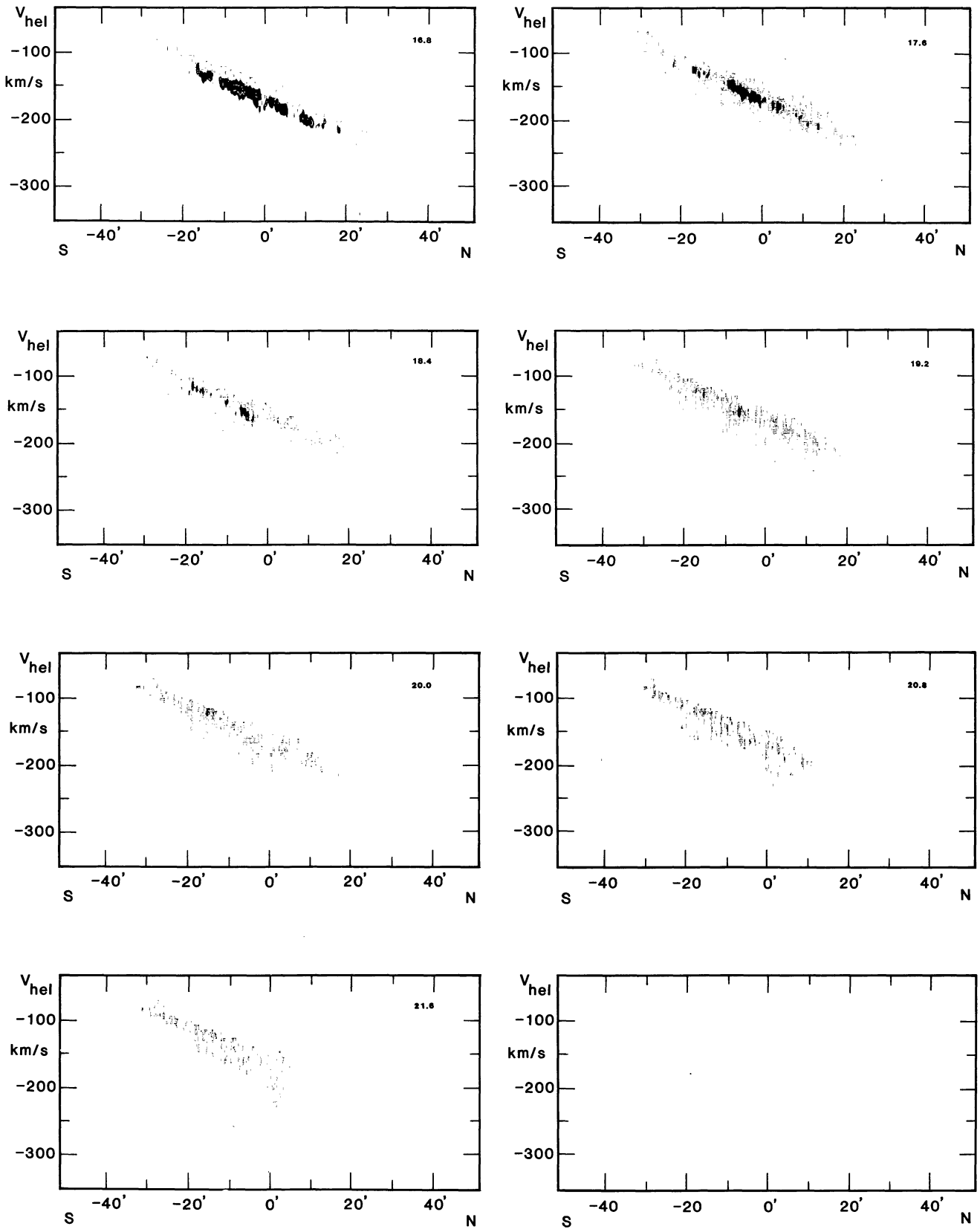

FIGURE 6 *(continued).*

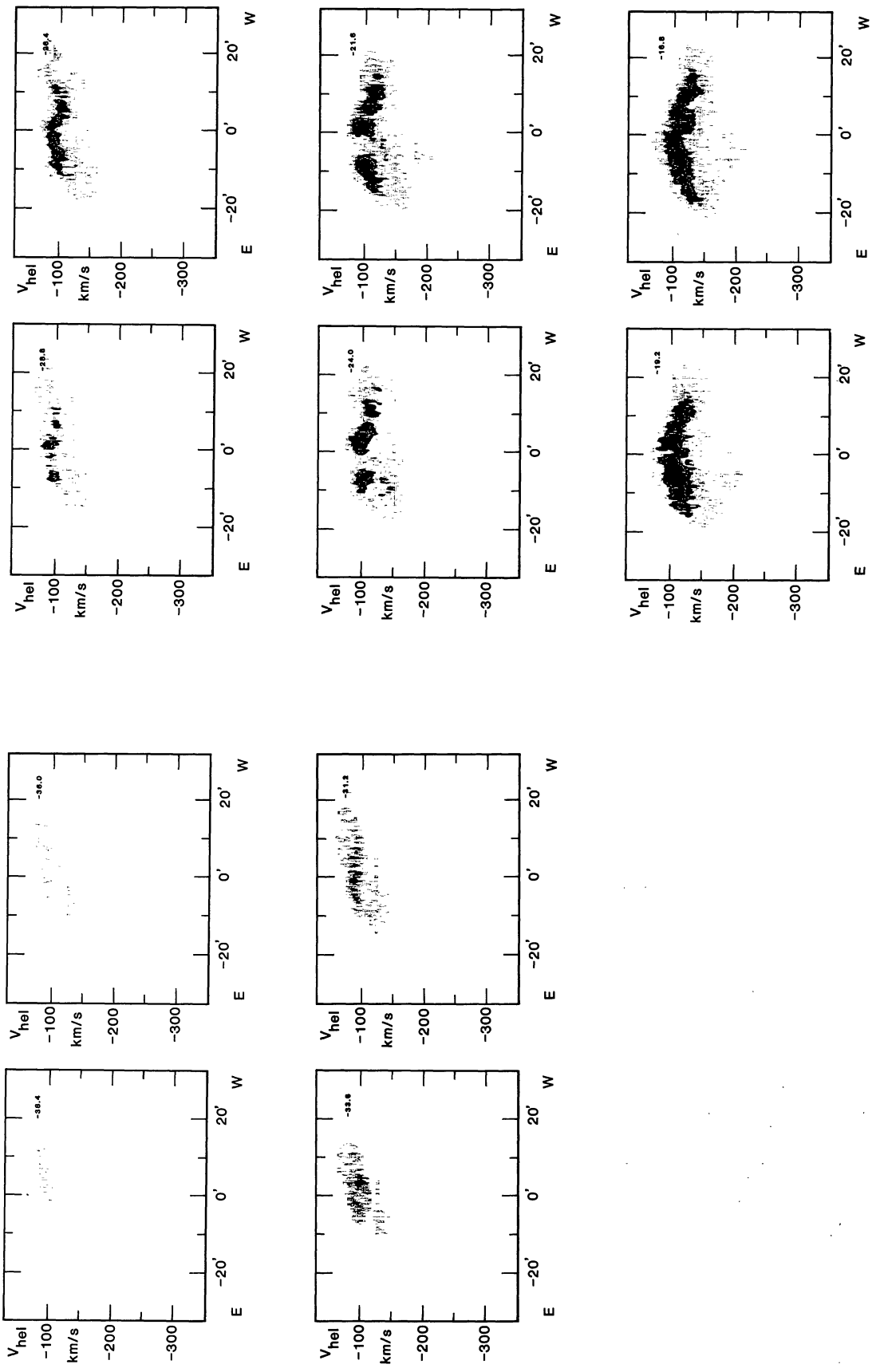

FIGURE 7. — Plots of position-velocity maps, alongs crosscuts perpendicular to the major axis of M33. The perpendicular distance from the minor axis is indicated at the top righthand corner of each frame. The contours and grey levels are drawn at the values indicated in the caption to figure 5.

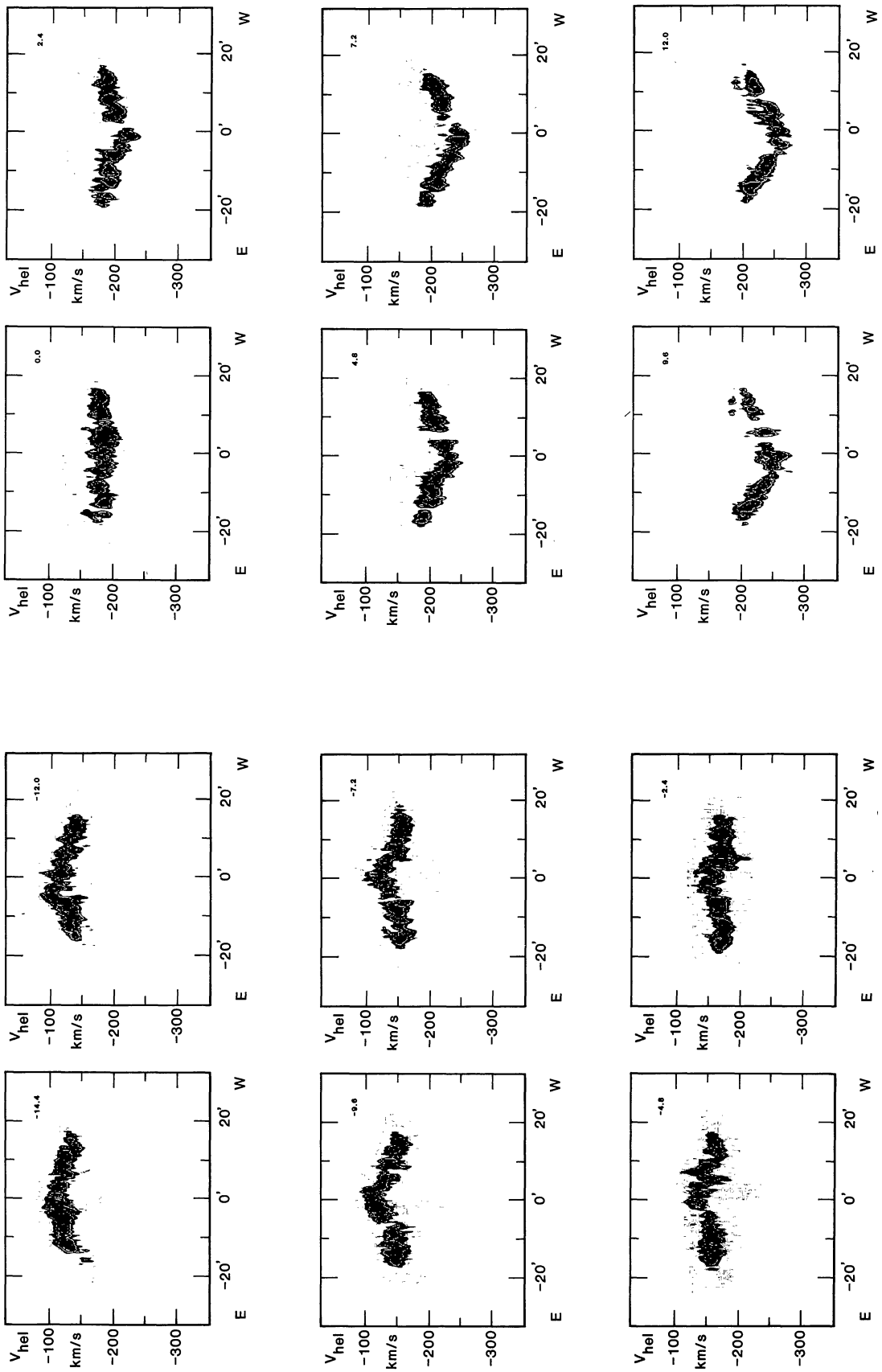

FIGURE 7 *(continued)*.

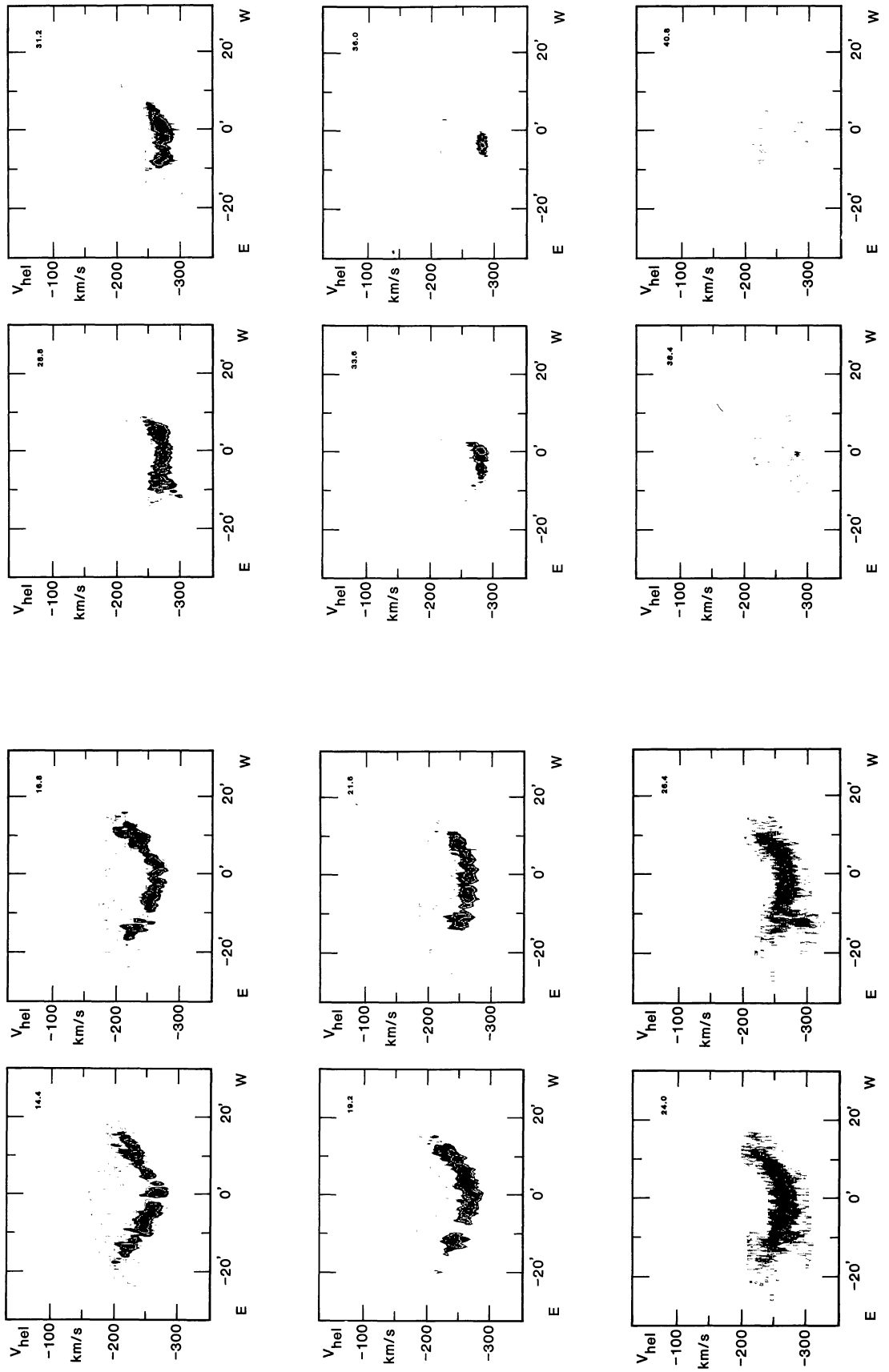

FIGURE 7 *(continued)*.

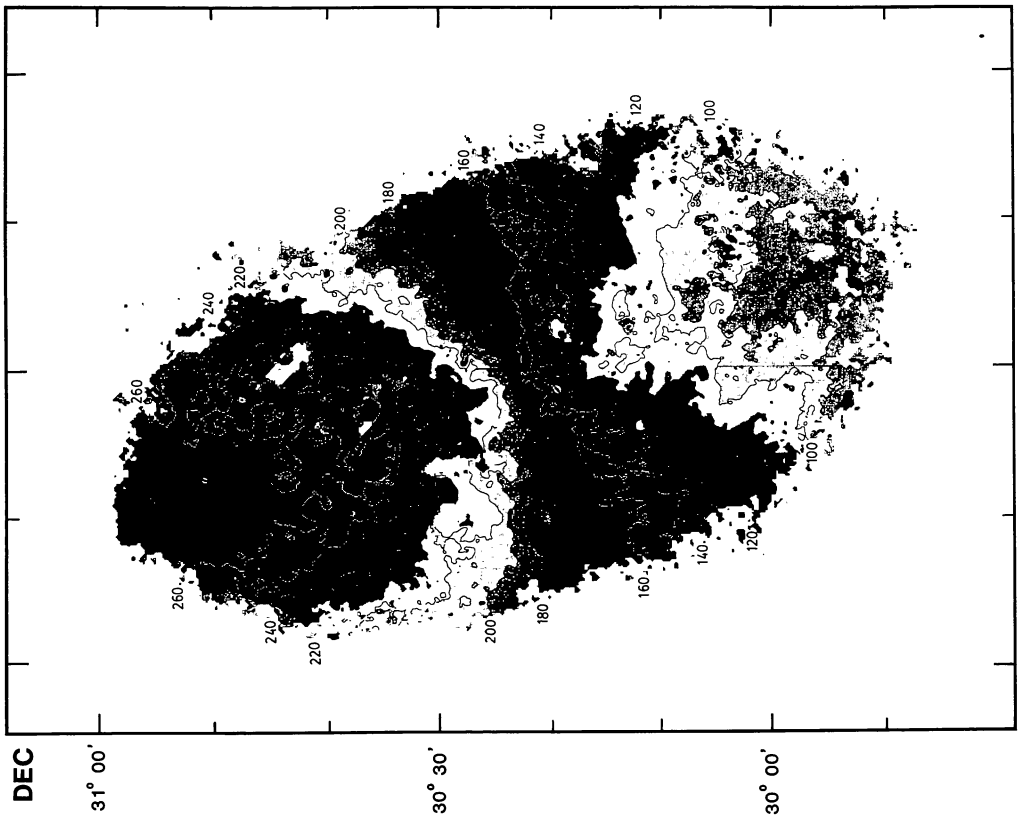

FIGURE 9. — Plot of the velocity field determined from this survey in the manner described in section 3. The contour interval is 10 km s^{-1} and contours range from − 320 km s^{-1} to − 50 km s^{-1}. The jump in the gray scale occurs at − 130 km s^{-1} and − 230 km s^{-1}. The numbers indicate the velocity in km s^{-1} at which the contour has been drawn.

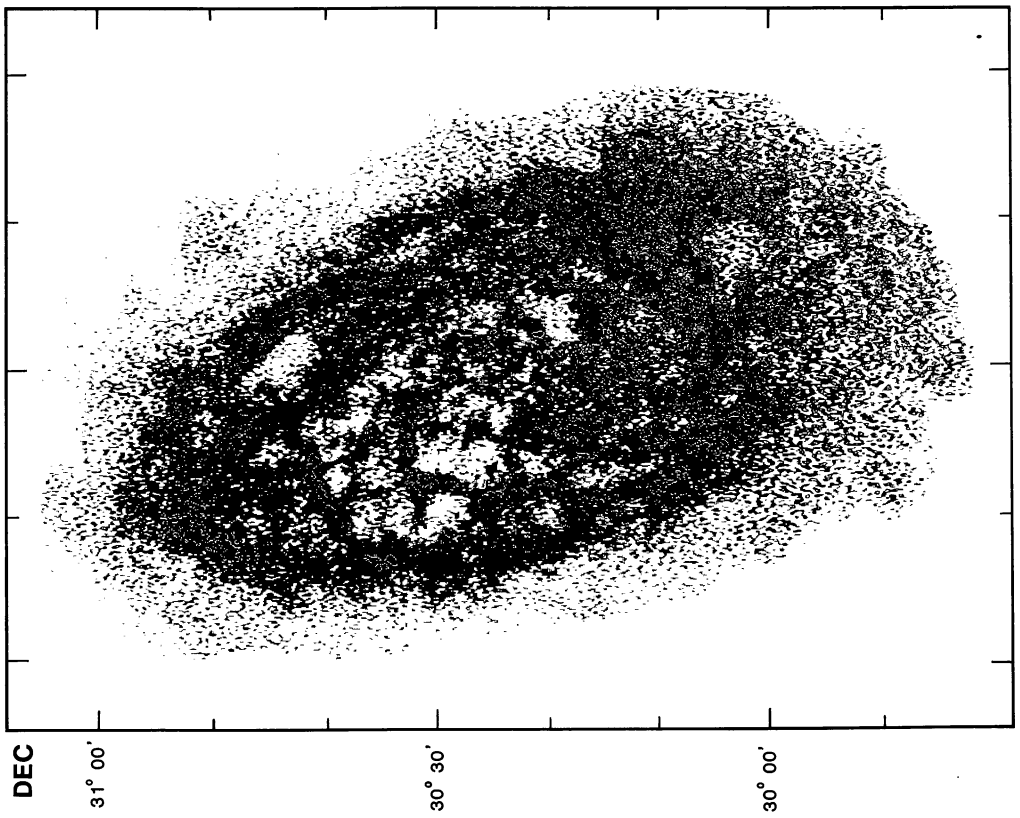

FIGURE 8. — Map of the HI column density distribution. The map is corrected for primary beam attenuation. The synthesized beam size is indicated in the lower righthand corner. The contours and grey levels are drawn at 93.4, 201.7, 442.8, 738.0, 1328.4, 2066.4, 2952.0 K km s^{-1}.

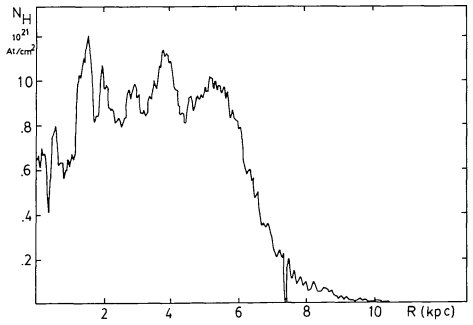

FIGURE 10. — Radial HI distribution derived from the hydrogen column density map by averaging in ellipses.